Overturning Pathways Control AMOC Weakening in CMIP6 Models

Jonathan A. Baker[1], Mike J. Bell[1], Laura C. Jackson[1], Richard Renshaw[1], Geoffrey K. Vallis[2], Andrew J. Watson[2], and Richard A. Wood[1]

[1]Met Office
[2]University of Exeter

February 27, 2023

Abstract

Future projections indicate the AMOC will weaken and shoal in response to global warming, but models disagree widely over the amount of weakening. We analyse projected AMOC weakening in 27 CMIP6 climate models, in terms of changes in three return pathways of the AMOC. The branch of the AMOC that returns through diffusive upwelling in the Indo-Pacific, but does not later upwell in the Southern Ocean, is particularly sensitive to warming, in part, because shallowing of the deep flow prevents it from entering the Indo-Pacific via the Southern Ocean. The present-day strength of this Indo-Pacific pathway provides a strong constraint on the projected AMOC weakening. However, estimates of this pathway using four observationally-based methods imply a wide range of AMOC weakening under the SSP5-8.5 scenario of 29% to 61% by 2100. Our results suggest that improved observational constraints on this pathway would substantially reduce uncertainty in 21st century AMOC decline.

Overturning Pathways Control AMOC Weakening in CMIP6 Models

Baker J.A.[1], Bell M.J. [1], Jackson L.C. [1], Renshaw R. [1], Vallis G.K. [2], Watson A.J. [2], Wood R.A. [1]

[1] Met Office, UK.

[2] University of Exeter, UK.

Corresponding author: Jonathan Baker (jonathan.baker@metoffice.gov.uk)

Index terms

4532 General circulation (1218, 1222); 4512 Currents; 4513 Decadal ocean variability (1616, 1635, 3305, 4215); 4568 Turbulence, diffusion, and mixing processes (4490)

Keywords

AMOC, overturning, pathways, weakening, constraint, CMIP6

Key Points:

- The magnitude of 21st century AMOC weakening in CMIP6 models is correlated with an AMOC pathway into the Indo-Pacific Ocean.
- The real-world "Indo-Pacific diffusive" AMOC pathway inferred from observation-based estimates was used to constrain future AMOC weakening.
- Under high-end greenhouse gas forcing, AMOC weakening based on this emergent constraint relationship ranges from 29% to 61% by 2100.

Abstract

Future projections indicate the AMOC will weaken and shoal in response to global warming, but models disagree widely over the amount of weakening. We analyse projected AMOC weakening in 27 CMIP6 climate models, in terms of changes in three return pathways of the AMOC. The branch of the AMOC that returns through diffusive upwelling in the Indo-Pacific, but does not later upwell in the Southern Ocean, is particularly sensitive to warming, in part, because shallowing of the deep flow prevents it from entering the Indo-Pacific via the Southern Ocean. The present-day strength of this Indo-Pacific pathway provides a strong constraint on the projected AMOC weakening. However, estimates of this pathway using four observationally-based methods imply a wide range of AMOC weakening under the SSP5-8.5 scenario of 29% to 61% by 2100. Our results suggest that improved observational constraints on this pathway would substantially reduce uncertainty in 21st century AMOC decline.

Plain Language Summary

Changes in the Atlantic Meridional Overturning Circulation (AMOC), an ocean conveyer belt that moves warm water northwards into the North Atlantic Ocean, would have wide-ranging impacts on our climate. The AMOC is predicted to weaken as the climate warms during the 21st century, but the extent of weakening differs among climate models. We show that AMOC weakening is greatest in models with a large exchange of water between the AMOC and the Indo-Pacific Ocean along a specific pathway. The magnitude of this ocean pathway, inferred from four observation-based estimates of the global overturning circulation, is uncertain. We use these estimates, and the relationship between the aforementioned ocean pathway and AMOC weakening across many climate models, to predict how the real-world AMOC will change. They indicate that by 2100 the AMOC will weaken by 29% to 61% under a high greenhouse gas emission scenario. This emphasises the importance of constraining the ocean's overturning pathways to reduce uncertainty in future AMOC weakening and to improve climate models so that they represent these pathways more realistically.

1. Introduction

The Atlantic Meridional Overturning Circulation (AMOC) is widely predicted to weaken over the 21st century (e.g., Cheng et al., 2013; Weijer et al., 2020), but the magnitude of this change is uncertain in the latest Coupled Model Intercomparison Project (CMIP6). Understanding the mechanisms responsible for the large inter-model spread is crucial to

predict the transient response of the AMOC to increased greenhouse gas concentrations. The ocean's overturning pathways are an important determinant of the equilibrium response of the AMOC to climate forcing (Baker et al., 2020, 2021; Nadeau & Jansen, 2020) and they may therefore also play a role in determining its transient response. We hypothesise that the wide range in the AMOC's transient response to climate forcing among CMIP6 models is due to differences in the historical magnitude of their overturning pathways.

Changes in the Meridional Overturning Circulation (MOC) influence global and regional climate change on seasonal to millennial timescales by changing the ocean's transport of heat, freshwater, and carbon (Buckley & Marshall, 2016; Rahmstorf, 2015; Weijer et al., 2019). How the AMOC changes over the 21st century will impact many aspects of the climate (Bellomo et al., 2021; Hu et al., 2020; Liu et al., 2020), so constraining its future response to warming is vital.

The most comprehensive predictions of future changes in climate are provided by CMIP6, a multi-model ensemble of climate simulations (Eyring et al., 2016; O'Neill et al., 2016). In model intercomparison projects, the weakening of the AMOC induced by increasing greenhouse gas (GHG) forcing tends to be greater in models with a stronger control AMOC, so its present-day strength can be used to constrain future weakening (e.g., Cheng et al., 2013; Gregory et al., 2005; Weaver et al., 2012; Weijer et al., 2020; Winton et al., 2014). Several mechanisms have been proposed to explain this dependence. These include the impact of northern sea-ice extent and its subsequent retreat on North Atlantic Ocean heat loss (Levermann et al., 2007), changes in the kinetic energy of the North Atlantic (Gregory & Tailleux, 2011), changes in Labrador Sea convection (Rugenstein et al., 2013), and North Atlantic salinity differences (Jackson et al., 2020). These arguments are based on differences in the mean state and response of the North Atlantic that ultimately affect North Atlantic convection. In contrast, we use the CMIP6 ensemble to investigate the cause of the inter-model spread in AMOC weakening and its dependence on the historical AMOC strength by analysing the model overturning pathways (e.g., Lumpkin & Speer, 2007; Talley, 2013) that return deep waters formed in the North Atlantic to their origin.

The pathways that return NADW to the surface in the present-day ocean either upwell in the Southern Ocean (SO) driven by the SO westerly winds (e.g.,Toggweiler & Samuels, 1998) or in the Atlantic and Indo-Pacific Oceans driven by diffusion (e.g., Munk & Wunsch, 1998). Diffusive upwelling in the Indo-Pacific Ocean may significantly affect the equilibrium state of

the global overturning circulation (Ferrari et al., 2017; Jones & Cessi, 2016; Newsom & Thompson, 2018; Thompson et al., 2016); however, its impact on shorter, transient timescales is less clear. Transient changes in the AMOC in response to GHG forcing are believed to be instigated by changes in the North Atlantic buoyancy forcing (Dixon et al., 1999; Stouffer et al., 2006), although the strengthening and poleward shift of the Southern Ocean westerly winds found under high-end warming scenarios in CMIP6 models (Deng et al., 2022) may also impact the AMOC. The equilibrium AMOC probably shoaled in cooler, glacial climates, decoupling the upper and lower cells of the MOC and thus isolating the AMOC from the Indo-Pacific Ocean (Baker et al., 2020, 2021; Ferrari et al., 2014; Nadeau & Jansen, 2020). The AMOC may also shoal in response to GHG forcing with its transient response investigated in idealised models (e.g., Bonan et al., 2022; Chang & Jansen, 2022; Sun et al., 2020). Sun et al. (2020) show that the Indo-Pacific overturning circulation responds rapidly to GHG forcing, weakening to compensate changes in the AMOC through communication between the North Atlantic and Indo-Pacific Oceans via wave processes. By analysing the overturning pathways under varying GHG forcing, we can infer the importance (if any) of Indo-Pacific and Southern Ocean processes on the transient response of the AMOC.

The main questions we seek to answer are:

- What are the historical overturning pathways in the CMIP6 ensemble and how do they change in a warmer climate?
- How does the transient weakening of the AMOC depend on the historical overturning pathways, and what mechanisms are responsible for these dependencies?
- Can we use estimates of the real-world overturning pathways to constrain future AMOC weakening?

2. Data and Methods

2.1. CMIP6 Models and observation-based data

We analyse the overturning pathways in the CMIP6 historical (1850-2014) simulation (Eyring et al., 2016) and in the Scenario Model Intercomparison Project (ScenarioMIP; O'Neill et al., 2016) experiments (2015-2100). The ScenarioMIP experiments represent different Shared Socioeconomic Pathways (SSP's; Riahi et al., 2017) that result in varying radiative forcing and thus warming by 2100. These range from low-end (SSP1-2.6 ("ssp126")) to high-end (SSP5-8.5 ("ssp585")) forcing scenarios. We focus on ssp585 since the AMOC response to forcing is greatest. The monthly-mean overturning mass

streamfunction (Griffies et al., 2016) is produced by 49 models for the historical simulation, 26 models for ssp126 and 27 models for ssp585 (Table S1). We analyse the overturning streamfunction in depth space, and in density space when it is available, using a single ensemble member from each model (Table S1). We average the monthly-mean overturning streamfunction over 1850-2014 in the historical simulation and over 2080-2100 in the ScenarioMIP experiments.

We estimate the real-world overturning pathways from three global ocean reanalyses that assimilate observations into an ocean model: "GloRanV14" (updated version of "GloSea5" e.g., Baker et al., 2022) over 2000-2021, the "Estimating the Circulation and Climate of the Ocean" (ECCOv4; Cessi, 2019; Forget et al., 2015) over 1992-2015 and a robust diagnostic simulation of Lee et al. (2019) that assimilates long-term averaged hydrographic data. We also use the MOC estimate from the inverse model of Lumpkin & Speer (2007) that uses hydrographic data measured over 1987-1996.

2.2. Method to separate the overturning pathways

We calculate the time-mean overturning pathways following the method of Baker et al. (2020, 2021) with a few modifications. We define the AMOC herein as the mid-depth cell in the Atlantic basin that is often referred to as the North Atlantic Deep Water (NADW) cell. The maximum strength of the AMOC in the North Atlantic is defined as "$AMOC_{max}$". We refer to each pathway (Table S3) of the MOC as a pathway of NADW, although the density of this water mass changes as it is transported through the ocean.

To separate the pathways, we use the zonally-averaged meridional overturning streamfunction in the Atlantic and Indo-Pacific basins, and in the Southern Ocean (SO), defined as all latitudes south of 34.5°S, we use the globally-integrated meridional overturning streamfunction (Figure 1). The dynamics of the SO are dominated by the effects of the SO winds, which generate an upper cell and indirectly strengthen a lower eddy-induced cell by tilting the SO isopycnals. We partition the AMOC transport southwards across 34.5°S into that advected into the upper and lower cells of the SO (Figure 1). The transport into the SO lower cell ("$NADW\_IP_{lower}$") must ultimately upwell in the Indo-Pacific basin, whereas that transported into the upper cell either upwells in the SO and returns to the Atlantic basin (the "Atlantic wind pathway"; "$NADW\_At_{wind}$") or it is transported by zonal flows into the Indo-Pacific basin ("$NADW\_IP_{upper}$"; not present in Figure 1 but we account for this pathway in our calculations). The total pathway into the Indo-Pacific basin either upwells diffusively in

this basin without later upwelling in the SO (the Indo-Pacific diffusive pathway; "NADW_IP$_{diffu}$") or it upwells initially via diffusion and later via the SO upper cell (the Indo-Pacific wind pathway; "NADW_IP$_{wind}$"). The total SO wind pathway ("NADW_wind$_{total}$") is equal to the sum of the Indo-Pacific and Atlantic wind pathways, and it is therefore equal to the total upwelling by the SO upper cell (Figure 1).

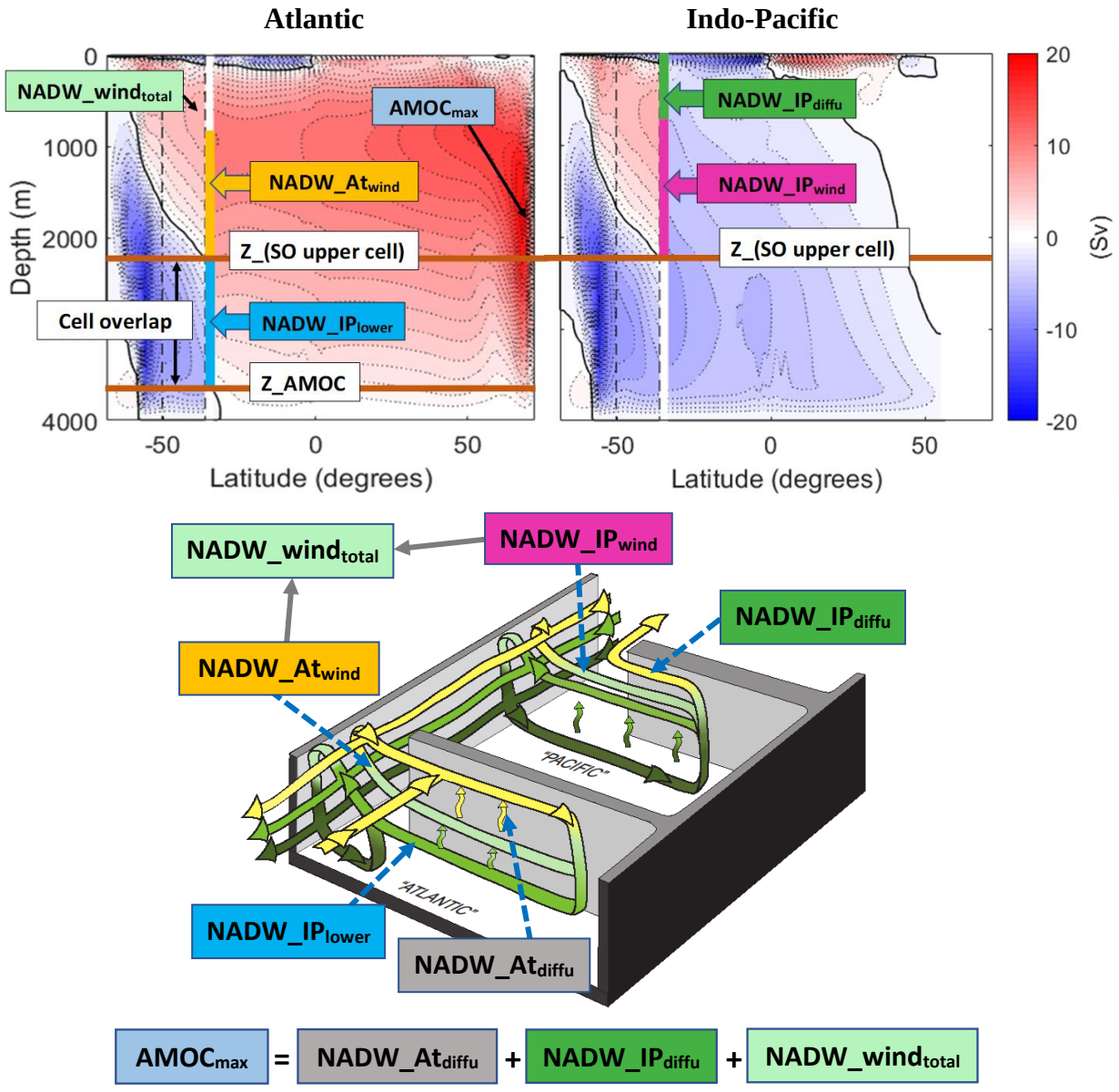

Figure 1. (upper) Meridional overturning streamfunction (Sverdrups (Sv); 2 Sv contours) from Baker et al. (2020; 2021), illustrating the method used to separate the overturning pathways. North of 34.5°S (right-hand vertical dashed lines), the streamfunction is plotted for the model Atlantic (left) and Indo-Pacific (right). The global-integrated streamfunction is plotted in the Southern Ocean. The solid black contour is the 0-Sv streamline. Each pathway, except "NADW_wind$_{total}$", is equal to the net volume of water flowing from the northern basin into the Southern Ocean over the depth of the associated coloured vertical line at 34.5°S. (lower) Illustration of the overturning pathways.

The Atlantic diffusive pathway ("NADW_At_{diffu}") upwells NADW in the Atlantic basin before returning northwards, that is, the streamlines of the AMOC are closed within the Atlantic basin. The sum of the three main pathways analysed; the Atlantic diffusive pathway ("NADW_At_{diffu}"), the total SO wind pathway ("NADW_$wind_{total}$") and the Indo-Pacific diffusive pathway ("NADW_IP_{diffu}"), are equal to "$AMOC_{max}$" (Figure 1 and Table S3). These pathways define the processes by which North Atlantic origin waters are returned to the surface; these waters either upwell in the Atlantic or Indo-Pacific basins via diffusion or they upwell in the SO via the SO winds. Further modifications to the method of Baker et al. (2020, 2021) and the equations used to calculate the pathways (eq. S1-S5) are described in the Supporting Information.

The overturning pathways are more accurately represented in density space since ocean currents tend to flow along isopycnals (Hallberg & Gnanadesikan, 2006). We compare the overturning pathways calculated in depth and density space in five models (Figure S1). Although there are quantitative differences in density space, we expect the qualitative findings of this study to remain valid (see Supporting Information).

3. Historical MOC and overturning pathways

3.1. MOC

We first examine the historical (1850-2014) overturning streamfunction and the associated overturning pathways. In all models, the Atlantic has a clockwise, mid-depth cell (i.e., the AMOC), whereas the Indo-Pacific has an expansive anti-clockwise cell. The historical AMOC strength ("$AMOC_{max}$") ranges from ~10 Sv to ~37 Sv, and there is significant inter-model spread in the overturning pathways (Figure 2, S2).

3.2. Absolute overturning pathways

Since the sum of the Atlantic and Indo-Pacific diffusive pathways and the total SO wind pathway are equal to "$AMOC_{max}$", we might expect the historical AMOC strength to correlate with the magnitude of each pathway. While the AMOC strength has a strong, positive correlation with the Atlantic and Indo-Pacific diffusive pathways, it is insignificantly ($p>0.05$) anti-correlated with the total SO wind pathway (Figure 2a-c). This is because there are a cluster of models with weak total SO wind pathways, yet strong AMOC's (left side of Figure 2b) because they have large Indo-Pacific diffusive pathways (right side of Figure 2c). The remaining models show a positive correlation between the AMOC strength and the total SO wind pathway**.**

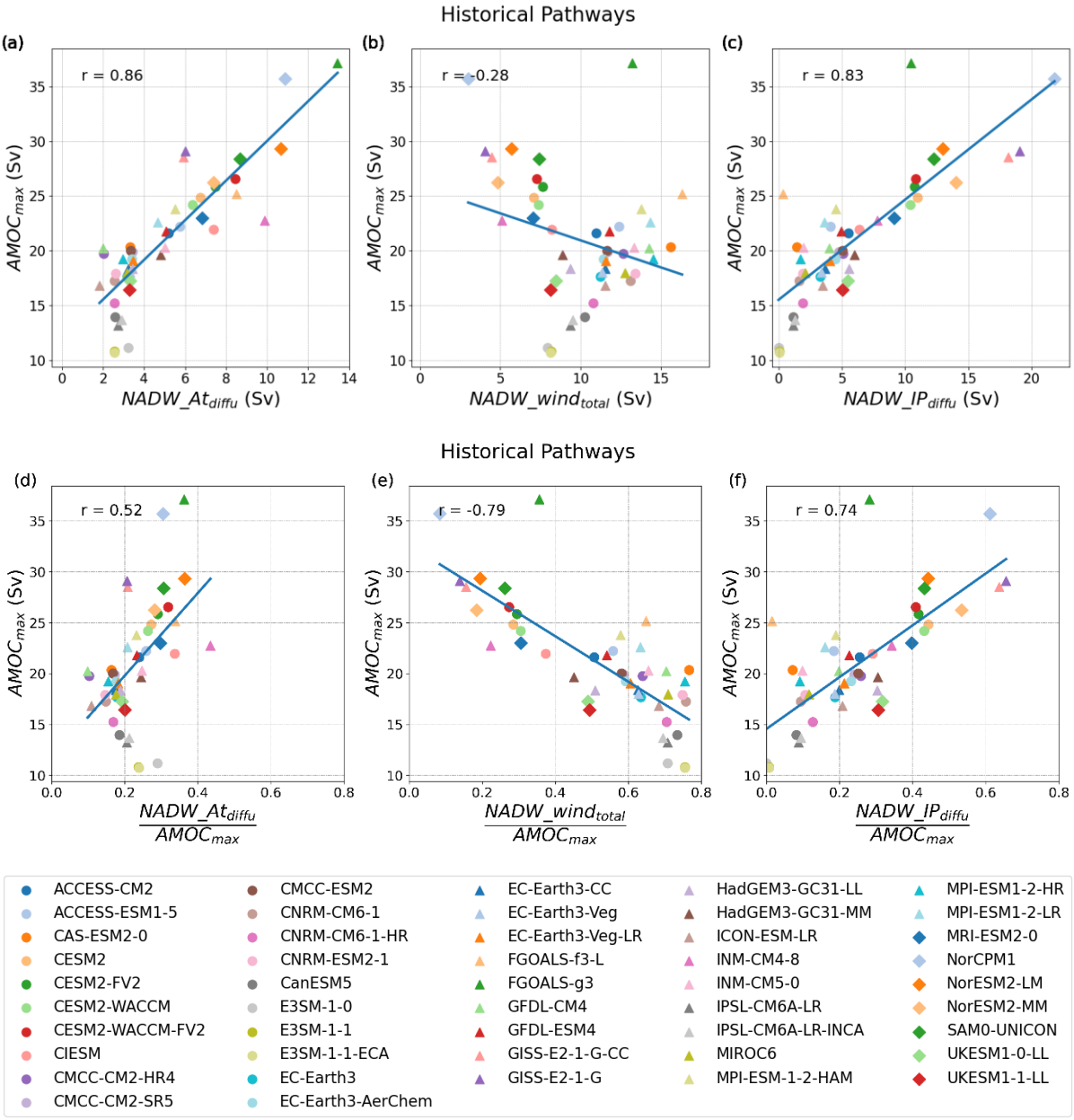

Figure 2. (upper) Overturning pathways and (lower) overturning pathways relative to the maximum AMOC strength in the North Atlantic, "$AMOC_{max}$", calculated in depth space and averaged over the historical simulation (1850-2100), plotted against "$AMOC_{max}$". The Atlantic diffusive pathway, "$NADW\_At_{diffu}$", the total SO wind pathway, "$NADW\_wind_{total}$" and the Indo-Pacific diffusive pathway, "$NADW\_IP_{diffu}$" are plotted. The line of best fit and the Pearson correlation coefficient are shown.

3.3. Relative overturning pathways

We also find similar relationships, but with lower correlations, between the historical AMOC strength and the overturning pathways relative to this AMOC strength i.e., the relative contribution of each pathway to "$AMOC_{max}$" (Figure 2d-e). However, the "relative" total SO wind pathway is significantly anti-correlated with AMOC strength. Thus, models with lower

"relative" total SO wind pathways tend to have stronger AMOC's due, in part, to reasons stated in Section 3.2. The "relative" total SO wind and Indo-Pacific diffusive pathways have similar ranges but opposing relationships with "$AMOC_{max}$" (Figure 2d,e). The ensemble-mean "relative" total SO wind pathway (55%) is greater than the ensemble-mean "relative" Indo-Pacific (22%) and Atlantic (23%) diffusive pathways (Figure 2d-f).

4. Transient response of AMOC and overturning pathways to warming

4.1. AMOC weakening

All warming scenarios in the CMIP6 ensemble predict a weakening of the AMOC over the 21st century, but there is a large inter-model variation. The AMOC weakens by 9%–42% (mean value of 24%) in ssp126 (Figure 3a) and by 21%–67% (mean value of 44%) in ssp585 by 2080-2100 (Figure 3d), relative to the historical (1850-2014) mean AMOC for each model. We also find that models with a stronger historical AMOC tend to have greater AMOC weakening (Figure 3a-d), in agreement with previous inter-model comparison studies (e.g., Weaver et al., 2012; Weijer et al., 2020; Winton et al., 2014). The strength of this relationship increases at higher rates of warming i.e., from ssp126 to ssp585. In addition to the AMOC weakening, the Indo-Pacific MOC also weakens (Figure S3), compensating changes in the AMOC (in agreement with Sun et al. (2020)).

4.2. Changes in the overturning pathways

We analyse the association between the magnitude of the historical overturning pathways and AMOC weakening in ssp585 (Figure 3e-g). Both the Atlantic and Indo-Pacific diffusive pathways are positively correlated with AMOC weakening (i.e., these pathways tend to be larger in models with greater weakening). In contrast, the total SO wind pathway is anti-correlated with AMOC weakening. The Indo-Pacific diffusive pathway explains 81% of the variance in AMOC weakening (i.e., r=0.90 in spp585; Figure 3g), notably higher than the 55% of the variance explained by the historical AMOC strength (i.e., r=0.74 in ssp585; Figure 3d). The AMOC weakening has a lower dependence on the Atlantic diffusive and total SO wind pathways (r=0.61 and r=-0.62 respectively), which therefore reduce the dependence of AMOC weakening on the historical AMOC strength**.** Thus, the primary reason for the

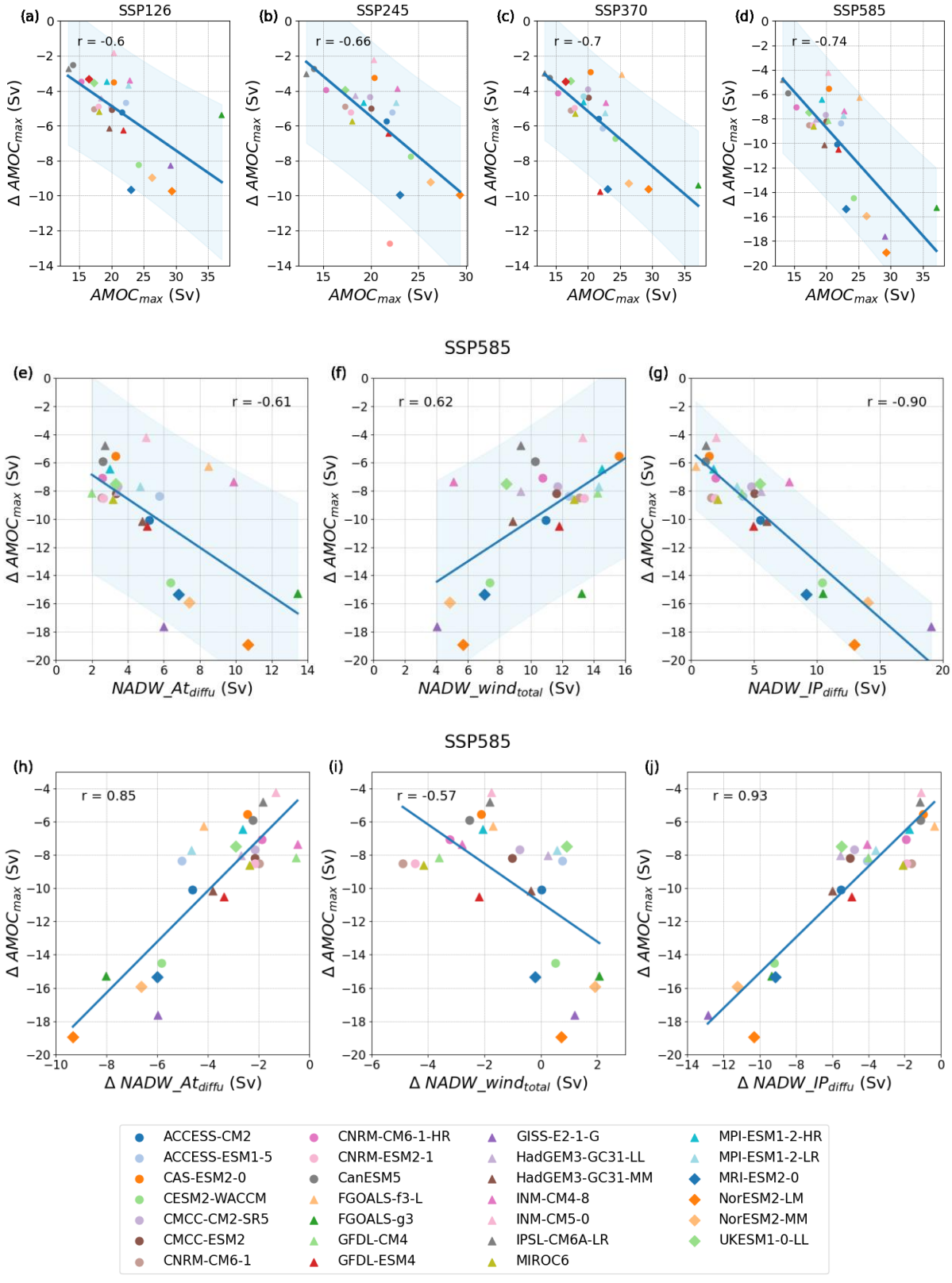

Figure 3. (upper panels) The historical average AMOC strength, "AMOC$_{max}$, plotted against the change in "AMOC$_{max}$" by 2080-2100 in (i) ssp126 (ii) ssp245 (iii) ssp370 and (iv) ssp585. (center panels) Historical overturning pathways and (lower panels) their change, plotted against the change in "AMOC$_{max}$" by 2080-2100 in ssp585. Blue shading represents the 95% prediction interval. Further details are specified in Figure 2.

strong dependence of AMOC weakening on the historical AMOC strength is its strong dependence on the Indo-Pacific diffusive pathway. The aforementioned correlation coefficients are lower for ssp126 than ssp585, but the AMOC weakening still has a higher correlation with the Indo-Pacific diffusive pathway (r=0.78, not shown) than with the historical AMOC strength (r=0.6; Figure 3a).

We now look at how the overturning pathways in ssp585 change over the 21st century (Figure 4) to understand why the AMOC weakening is strongly dependent on the Indo-Pacific diffusive pathway (and less dependent on the other pathways). Although the AMOC weakens in all models, the rate and magnitude of weakening vary greatly (Figure 4a,e). By 2100, all models predict a decrease in the Indo-Pacific and Atlantic diffusive pathways, but the total SO wind pathway has a mixed response (Figure 4b-d,f-h). This pathway typically contributes little to the change in AMOC strength (Figure 4c,g) so has little impact on the relationship between the Indo-Pacific diffusive pathway and AMOC weakening. This is probably because changes in the SO winds are too small to weaken the SO upper cell and because the SO overturning is slow to respond to changes in the AMOC (Chang & Jansen, 2022; Sun et al., 2020). By 2100, the decrease in the Indo-Pacific diffusive pathway has a large inter-model spread (~1 Sv to ~13 Sv), whereas the Atlantic diffusive pathway tends to have a smaller decrease (Figure 4). Changes in these pathways are highly correlated (r=0.76, not shown).

The weakening of the AMOC is strongly correlated with decreases in the Atlantic and Indo-Pacific diffusive pathways (Figure 3h,j). In contrast, changes in the total SO wind pathway are weakly anti-correlated with AMOC weakening due to the subset of models with a strong Indo-Pacific diffusive pathway weakening most despite little change in their total SO wind pathways (Figure 3i). We also find changes in the Indo-Pacific diffusive pathway are almost inversely proportional to its historical magnitude (r=-0.97; not shown), whereas changes in the Atlantic and total SO wind pathways are less dependent on their historical magnitudes (r=-0.7 and r=-0.45 respectively).

4.3. Mechanisms

The almost proportional relationship between the historical Indo-Pacific diffusive pathway and its decrease by 2080-2100 is due, in part, to this pathway weakening to zero in many models during the 21st century (Figure 4d). The historical magnitude of this pathway therefore sets an upper limit on its weakening and constrains the AMOC's decline. Thus, while reduced North Atlantic convection probably causes the AMOC weakening, the

magnitude of decline is modulated by the magnitude of the Indo-Pacific diffusive pathway, with changes communicated rapidly via wave processes (Sun et al., 2020). This pathway decreases, in part, because the "cell overlap" between the AMOC and the SO lower cell decreases in response to GHG forcing, reducing the main pathway for NADW to enter the Indo-Pacific Ocean (Figure S3; see Baker et al., 2020, 2021; Nadeau & Jansen, 2020).

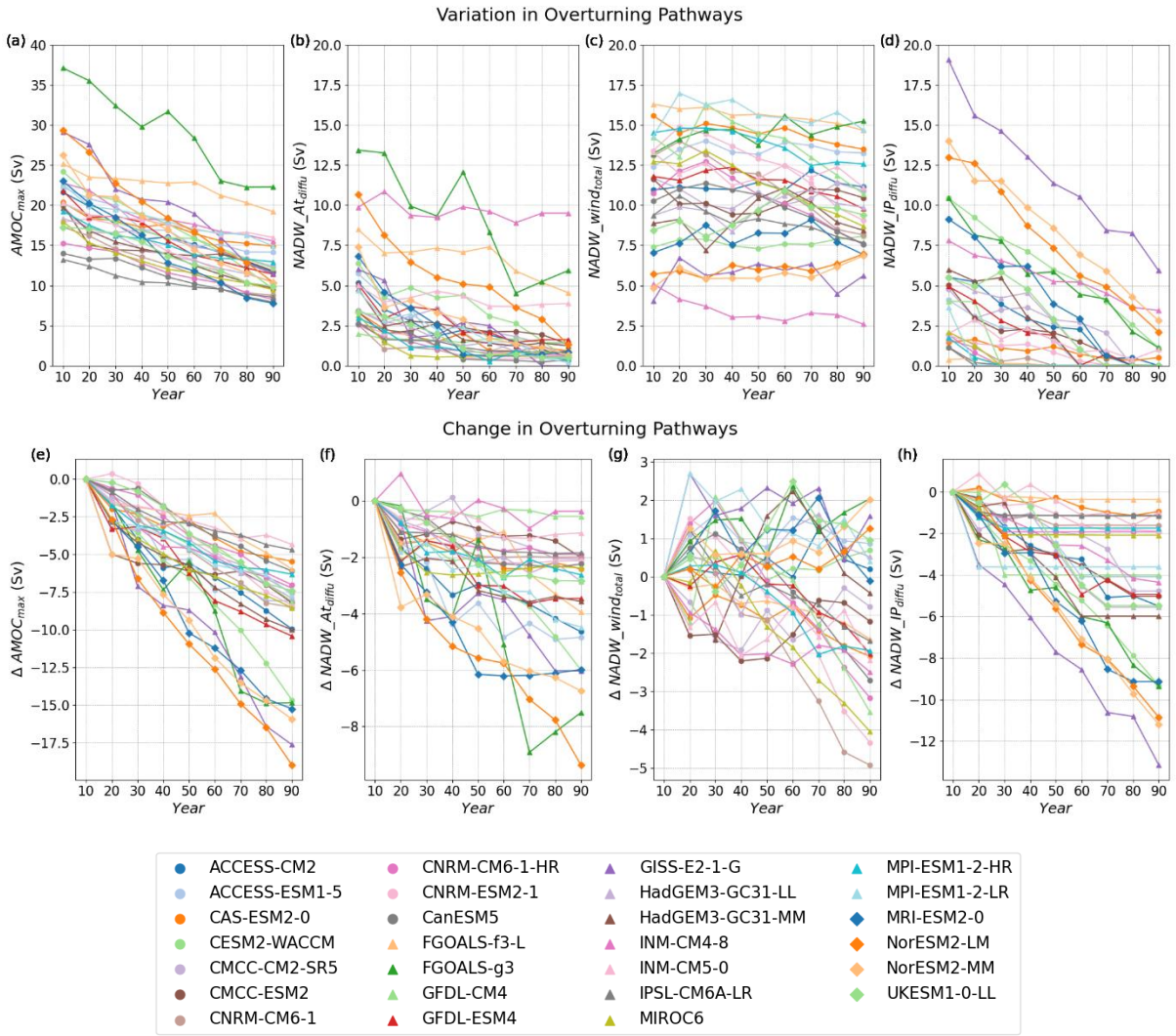

Figure 4. Timeseries of the AMOC strength and overturning pathways showing (upper panels) their absolute magnitudes, and (lower panels) the change in their magnitudes from the historical average (1850-2014). The historical average is labelled as 2010 ("10") with average values in "ssp585" calculated in 10-year intervals from 2015-2095 (labelled "20" to "90").

5. Constraining future AMOC weakening

Since the weakening of the AMOC is strongly related to the magnitude of the historical Indo-Pacific diffusive pathway, we use this emergent constraint relationship to predict future weakening of the real-world AMOC. Using the AMOC strength and overturning pathways inferred from observation-based MOC estimates (Table S2), the emergent constraint

relationship (Figure 3f) predicts large differences in AMOC decline by 2080-2100 under ssp585 forcing; 29% (range of 8%–50% from the 95% prediction interval in Figure 3f) from ECCOv4, 35% (14%–56%) from an inverse model estimate (Lumpkin & Speer, 2007), 41% (26%–56%) from a robust diagnostic simulation (Lee et al., 2019) and 61% (41%–81%) from GloRanV14 (Table S2). Under ssp126 forcing, the emergent constraint predicts a weaker AMOC decline for each observation-based estimate, ranging from 17% to 32% (Table S2).

Although the prediction intervals of the emergent constraint relationship are large (Figure 3f), they are significantly smaller than the equivalent analysis using the historical AMOC strength to constrain the weakening (Figure 3d). Each of the observation-based estimates of AMOC strength (except the robust diagnostic simulation) and a direct observational estimate at 26.5°N of 16.9 Sv (Moat et al., 2022) imply a weakening under ssp585 forcing of ~41% (6%–76%) by 2100. Despite high confidence in the AMOC strength observed at 26.5°N, AMOC weakening constrained by this estimate is highly uncertain. Thus, even though the magnitude of the Indo-Pacific diffusive pathway is uncertain, AMOC weakening based on this pathway has a comparable uncertainty (8%–81%) to that based on the AMOC strength. Between observation-based estimates, their South Atlantic transports are similar, but their total SO wind pathways and thus Indo-Pacific diffusive pathways differ (Table S2). Reducing uncertainty in the strength of the SO upper cell at 34.5°S and thus in these pathways would increase confidence in estimates of future AMOC decline.

6. Discussion and Conclusions

The response of the AMOC to GHG forcing in the CMIP6 multi-model ensemble is uncertain. Under low-end forcing (SSP1-2.6), by 2080-2100 the AMOC in each model weakens on average by 24% (range of 9%–42% across the ensemble) relative to its historical mean AMOC, while under high-end forcing (SSP5-8.5), the average weakening increases to 44% (range of 21%–67%). We show that the partition of the historical (1850-2014) overturning pathways largely determines how the AMOC responds to future climate forcing. Specifically, the historical pathway of North Atlantic origin waters that upwells diffusively in the Indo-Pacific Ocean but is not later upwelled in the Southern Ocean (SO) is strongly related to the weakening of the AMOC. Under high-end forcing, this historical Indo-Pacific diffusive pathway explains 81% of the variance in the AMOC weakening across the ensemble compared to only 55% that is explained by the historical AMOC strength. This emergent constraint relationship on AMOC weakening can be used to predict future changes

in the AMOC. Due to large uncertainty in observation-based estimates of the real-world Indo-Pacific diffusive pathway, they imply a wide range of AMOC weakening by 2080-2100 of 17%–32% (best estimates) under SSP1-2.6 forcing and of 29%–61% under SSP5-8.5 forcing.

Mechanisms proposed to explain the association between the weakening of the AMOC and its historical strength (e.g., Cheng et al., 2013; Weaver et al., 2012; Weijer et al., 2020) largely focus on the mean state of the North Atlantic (e.g., Jackson et al., 2020; Levermann et al., 2007). We argue that because AMOC weakening has a stronger dependence on the Indo-Pacific diffusive pathway than the historical AMOC strength, these North Atlantic based mechanisms may not fully explain this relationship. Although changes in North Atlantic convection likely cause the AMOC to shoal and weaken, the magnitude of this weakening is largely controlled by the magnitude of the Indo-Pacific diffusive pathway.

As the AMOC shoals, the "cell overlap" between the AMOC and the SO lower cell decreases, reducing the pathway into the Indo-Pacific Ocean (e.g., Baker et al., 2020, 2021; Nadeau & Jansen, 2020). The weakening of the AMOC is strongly dependent on the historical magnitude of the Indo-Pacific diffusive pathway, in part, because its magnitude acts as an upper limit on its decrease. Changes in the pathway that upwells in the Atlantic are also strongly related to changes in the Indo-Pacific diffusive pathway, whereas the pathway that upwells North Atlantic origin waters via the SO upper cell has only a weak response.

The structure and strength of the AMOC is thought to be set by the buoyancy forcing, the vertical diffusivity, the SO wind stress and mesoscale eddies, among other factors (Bellomo et al., 2021). The historical overturning pathways are therefore dependent on these model processes and forcings. Thus, accurately representing these processes in models is crucial to obtain a historical MOC and AMOC response that is realistic. Improved observational estimates of the real-world overturning pathways would reduce uncertainty in our prediction of AMOC weakening. They may also suggest how climate models can improve their representation of the historical MOC and thus changes in the AMOC, which could also improve their oceanic transports of heat, salinity and carbon (e.g., Aldama-Campino et al., 2020; Heuzé, 2021; Sun et al., 2022). Future research could attempt to understand the cause of the large inter-model spread in the historical overturning pathways and AMOC strength.

Acknowledgements

JAB, LCJ and RAW were supported by the European Union's Horizon 2020 research and innovation programme (grant no. 820970, TiPES project). LCJ, MJB and RAW were supported by the Met Office Hadley Centre Climate Programme funded by BEIS.

Open Research

The CMIP6 data used in this study is available from ESGF (https://esgf-index1.ceda.ac.uk/search/cmip6-ceda/) with references listed in Table S1. MOC estimates from ECCOv4, a robust diagnostic simulation and an inverse model were taken from Cessi (2019), Lee et al., 2019 and Lumpkin & Speer (2007) respectively. MOC estimates from GloRanV14 (funded by the E.U. Copernicus Marine Service) are available through Zenodo: https://doi.org/10.5281/zenodo.7649266 (Baker and Renshaw, 2023).

References

Aldama-Campino, A., Fransner, F., Ödalen, M., Groeskamp, S., Yool, A., Döös, K., & Nycander, J. (2020). Meridional Ocean Carbon Transport. *Global Biogeochemical Cycles*, *34*(9), e2019GB006336. https://doi.org/10.1029/2019GB006336

Baker, J. A., Watson, A. J., & Vallis, G. K. (2020). Meridional overturning circulation in a multibasin model. Part i: Dependence on southern ocean buoyancy forcing. *Journal of Physical Oceanography*, *50*(5), 1159–1178. https://doi.org/10.1175/JPO-D-19-0135.1

Baker, J. A., Watson, A. J., & Vallis, G. K. (2021). Meridional Overturning Circulation in a Multibasin Model. Part II: Sensitivity to Diffusivity and Wind in Warm and Cool Climates. *Journal of Physical Oceanography*, *51*(6), 1813–1828. https://doi.org/10.1175/JPO-D-20-0121.1

Bellomo, K., Angeloni, M., Corti, S., & von Hardenberg, J. (2021). Future climate change shaped by inter-model differences in Atlantic meridional overturning circulation response. *Nature Communications 2021 12:1*, *12*(1), 1–10. https://doi.org/10.1038/s41467-021-24015-w

Bonan, D. B., Thompson, A. F., Newsom, E. R., Sun, S., & Rugenstein, M. (2022). Transient and Equilibrium Responses of the Atlantic Overturning Circulation to Warming in Coupled Climate Models: The Role of Temperature and Salinity. *Journal of Climate*, *35*(15), 5173–5193. https://doi.org/10.1175/jcli-d-21-0912.1

Buckley, M. W., & Marshall, J. (2016). Observations, inferences, and mechanisms of the Atlantic Meridional Overturning Circulation: A review. *Reviews of Geophysics*, *54*(1), 5–63. https://doi.org/10.1002/2015RG000493

Cessi, P. (2019). The Global Overturning Circulation. *Https://Doi.Org/10.1146/Annurev-Marine-010318-095241*, *11*, 249–270. https://doi.org/10.1146/ANNUREV-MARINE-010318-095241

Chang, C.-Y., & Jansen, M. F. (2022). The time-dependent response of a two-basin ocean to a sudden surface temperature change. *Journal of Climate*, 1–34. https://doi.org/10.1175/jcli-d-21-0821.1

Cheng, W., Chiang, J. C. H., & Zhang, D. (2013). Atlantic Meridional Overturning Circulation (AMOC) in CMIP5 Models: RCP and Historical Simulations. *Journal of Climate*, *26*(18), 7187–7197. https://doi.org/10.1175/JCLI-D-12-00496.1

Deng, K., Azorin-Molina, C., Yang, S., Hu, C., Zhang, G., Minola, L., & Chen, D. (2022). Changes of Southern Hemisphere westerlies in the future warming climate. *Atmospheric Research*, *270*, 106040. https://doi.org/10.1016/J.ATMOSRES.2022.106040

Dixon, K. W., Delworth, T. L., Spelman, M. J., & Stouffer, R. J. (1999). The influence of transient surface fluxes on North Atlantic overturning in a coupled GCM Climate Change Experiment. *Geophysical Research Letters*, *26*(17), 2749–2752. https://doi.org/10.1029/1999GL900571

Eyring, V., Bony, S., Meehl, G. A., Senior, C. A., Stevens, B., Stouffer, R. J., & Taylor, K. E. (1937). Overview of the Coupled Model Intercomparison Project Phase 6 (CMIP6) experimental design and organization. *Geosci. Model Dev*, *9*. https://doi.org/10.5194/gmd-9-1937-2016

Ferrari, R., Jansen, M. F., Adkins, J. F., Burke, A., Stewart, A. L., & Thompson, A. F. (2014). Antarctic sea ice control on ocean circulation in present and glacial climates. *Proceedings of the National Academy of Sciences of the United States of America*, *111*(24), 8753–8758. https://doi.org/10.1073/PNAS.1323922111/SUPPL_FILE/PNAS.201323922SI.PDF

Ferrari, R., Nadeau L-P, Marshall, D., Allison, L. C., & Johnson, H. L. (2017). A Model of the Ocean Overturning Circulation with Two Closed Basins and a Reentrant Channel. *J. Phys. Oceanogr.*, *47*, 2887–2906. https://doi.org/10.1175/JPO-D-16-0223.1

Forget, G., Campin, J. M., Heimbach, P., Hill, C. N., Ponte, R. M., & Wunsch, C. (2015). ECCO version 4: An integrated framework for non-linear inverse modeling and global ocean state estimation. *Geoscientific Model Development*, *8*(10), 3071–3104. https://doi.org/10.5194/GMD-8-3071-2015

Gregory, J. M., Dixon, K. W., Stouffer, R. J., Weaver, A. J., Driesschaert, E., Eby, M., Fichefet, T., Hasumi, H., Hu, A., Jungclaus, J. H., Kamenkovich, I. v, Levermann, A., Montoya, M., Murakami, S., Nawrath, S., Oka, A., Sokolov, A. P., & Thorpe, R. B. (2005). *A model intercomparison of changes in the Atlantic thermohaline circulation in response to increasing atmospheric CO<subscr>2</subscr> concentration*. https://doi.org/10.1029/2005GL023209

Gregory, J. M., & Tailleux, R. (2011). Kinetic energy analysis of the response of the Atlantic meridional overturning circulation to CO2-forced climate change. *Climate Dynamics*, *37*(5), 893–914. https://doi.org/10.1007/S00382-010-0847-6/FIGURES/11

Griffies, S. M., Danabasoglu, G., Durack, P. J., Adcroft, A. J., Balaji, V., Böning, C. W., Chassignet, E. P., Curchitser, E., Deshayes, J., Drange, H., Fox-Kemper, B., Gleckler, P. J., Gregory, J. M., Haak, H., Hallberg, R. W., Heimbach, P., Hewitt, H. T., Holland, D. M., Ilyina, T., … Yeager, S. G. (2016). OMIP contribution to CMIP6: Experimental and diagnostic protocol for the physical component of the Ocean Model Intercomparison Project. *Geoscientific Model Development*, *9*(9), 3231–3296. https://doi.org/10.5194/GMD-9-3231-2016

Hallberg, R., & Gnanadesikan, A. (2006). The Role of Eddies in Determining the Structure and Response of the Wind-Driven Southern Hemisphere Overturning: Results from the Modeling Eddies in the Southern Ocean (MESO) Project. *Journal of Physical Oceanography*, *36*(12), 2232–2252. https://doi.org/10.1175/JPO2980.1

458 Heuzé, C. (2021). Antarctic Bottom Water and North Atlantic Deep Water in CMIP6 models. *Ocean*
459 *Science*, *17*(1), 59–90. https://doi.org/10.5194/os-17-59-2021

460 Hu, A., van Roekel, L., Weijer, W., Garuba, O. A., Cheng, W., & Nadiga, B. T. (2020). Role of AMOC in
461 Transient Climate Response to Greenhouse Gas Forcing in Two Coupled Models. *Journal of*
462 *Climate*, *33*(14), 5845–5859. https://doi.org/10.1175/JCLI-D-19-1027.1

463 Jackson, L. C., Roberts, M. J., Hewitt, H. T., Iovino, D., Koenigk, T., Meccia, V. L., Roberts, C. D.,
464 Ruprich-Robert, Y., & Wood, R. A. (2020). Impact of ocean resolution and mean state on the
465 rate of AMOC weakening. *Climate Dynamics*, *55*(7–8), 1711–1732.
466 https://doi.org/10.1007/s00382-020-05345-9

467 Jones, C. S., & Cessi, P. (2016). Interbasin Transport of the Meridional Overturning Circulation.
468 *Journal of Physical Oceanography*, *46*(4), 1157–1169. https://doi.org/10.1175/JPO-D-15-0197.1

469 Lee, S. K., Lumpkin, R., Baringer, M. O., Meinen, C. S., Goes, M., Dong, S., Lopez, H., & Yeager, S. G.
470 (2019). Global Meridional Overturning Circulation Inferred From a Data-Constrained Ocean &
471 Sea-Ice Model. *Geophysical Research Letters*, *46*(3), 1521–1530.
472 https://doi.org/10.1029/2018GL080940

473 Levermann, A., Mignot, J., Nawrath, S., & Rahmstorf, S. (2007). *The Role of Northern Sea Ice Cover*
474 *for the Weakening of the Thermohaline Circulation under Global Warming*.
475 https://doi.org/10.1175/JCLI4232.1

476 Liu, W., Fedorov, A. v., Xie, S. P., & Hu, S. (2020). Climate impacts of a weakened Atlantic meridional
477 overturning circulation in a warming climate. *Science Advances*, *6*(26).
478 https://doi.org/10.1126/SCIADV.AAZ4876/SUPPL_FILE/AAZ4876_SM.PDF

479 Lumpkin, R., & Speer, K. (2007). Global Ocean Meridional Overturning. *Journal of Physical*
480 *Oceanography*, *37*(10), 2550–2562. https://doi.org/10.1175/JPO3130.1

481 Menary, M. B., Hodson, D. L. R., Robson, J. I., Sutton, R. T., Wood, R. A., & Hunt, J. A. (2015).
482 Exploring the impact of CMIP5 model biases on the simulation of North Atlantic decadal
483 variability. *Geophysical Research Letters*, *42*(14), 5926–5934.
484 https://doi.org/10.1002/2015GL064360

485 Munk, W., & Wunsch, C. (1998). Abyssal recipes II: energetics of tidal and wind mixing. *Deep Sea*
486 *Research Part I: Oceanographic Research Papers*, *45*(12), 1977–2010.
487 https://doi.org/10.1016/S0967-0637(98)00070-3

488 Nadeau, L. P., & Jansen, M. F. (2020). Overturning Circulation Pathways in a Two-Basin Ocean Model.
489 *Journal of Physical Oceanography*, *50*(8), 2105–2122. https://doi.org/10.1175/JPO-D-20-0034.1

490 Newsom, E. R., & Thompson, A. F. (2018). Reassessing the Role of the Indo-Pacific in the Ocean's
491 Global Overturning Circulation. *Geophysical Research Letters*, *45*(22), 12,422-12,431.
492 https://doi.org/10.1029/2018GL080350

493 O'Neill, B. C., Tebaldi, C., van Vuuren, D. P., Eyring, V., Friedlingstein, P., Hurtt, G., Knutti, R., Kriegler,
494 E., Lamarque, J.-F., Lowe, J., Meehl, G. A., Moss, R., Riahi, K., & Sanderson, B. M. (2016). The
495 Scenario Model Intercomparison Project (ScenarioMIP) for CMIP6. *Geosci. Model Dev*, *9*, 3461–
496 3482. https://doi.org/10.5194/gmd-9-3461-2016

Rahmstorf, S. (2015). Exceptional twentieth-century slowdown in Atlantic Ocean overturning circulation. *Nat. Clim. Chang.*, *5*(5), 475–480. https://doi.org/10.1038/nclimate2554

Riahi, K., van Vuuren, D. P., Kriegler, E., Edmonds, J., O'Neill, B. C., Fujimori, S., Bauer, N., Calvin, K., Dellink, R., Fricko, O., Lutz, W., Popp, A., Cuaresma, J. C., KC, S., Leimbach, M., Jiang, L., Kram, T., Rao, S., Emmerling, J., … Tavoni, M. (2017). The Shared Socioeconomic Pathways and their energy, land use, and greenhouse gas emissions implications: An overview. *Global Environmental Change*, *42*, 153–168. https://doi.org/10.1016/J.GLOENVCHA.2016.05.009

Rugenstein, M. A. A., Winton, M., Stouffer, R. J., Griffies, S. M., & Hallberg, R. (2013). Northern High-Latitude Heat Budget Decomposition and Transient Warming. *Journal of Climate*, *26*(2), 609–621. https://doi.org/10.1175/JCLI-D-11-00695.1

Schmittner, A., Latif, M., & Schneider, B. (2005). Model projections of the North Atlantic thermohaline circulation for the 21st century assessed by observations. *Geophysical Research Letters*, *32*(23), 1–4. https://doi.org/10.1029/2005GL024368

Stouffer, R. J., Yin, J., Gregory, J. M., Dixon, K. W., Spelman, M. J., Hurlin, W., Weaver, A. J., Eby, M., Flato, G. M., Hasumi, H., Hu, A., Jungclaus, J. H., Kamenkovich, I. v., Levermann, A., Montoya, M., Murakami, S., Nawrath, S., Oka, A., Peltier, W. R., … Weber, S. L. (2006). Investigating the Causes of the Response of the Thermohaline Circulation to Past and Future Climate Changes. *Journal of Climate*, *19*(8), 1365–1387. https://doi.org/10.1175/JCLI3689.1

Sun, S., Thompson, A. F., & Eisenman, I. (2020). Transient Overturning Compensation between Atlantic and Indo-Pacific Basins. *Journal of Physical Oceanography*, *50*(8), 2151–2172. https://doi.org/10.1175/JPO-D-20-0060.1

Sun, S., Thompson, A. F., Xie, S. P., & Long, S. M. (2022). Indo-Pacific Warming Induced by a Weakening of the Atlantic Meridional Overturning Circulation. *Journal of Climate*, *35*(2), 815–832. https://doi.org/10.1175/JCLI-D-21-0346.1

Talley, L. D. (2013). Closure of the global overturning circulation through the Indian, Pacific, and southern oceans. *Oceanography*, *26*(1), 80–97. https://doi.org/10.5670/OCEANOG.2013.07

Thompson, A. F., Stewart, A. L., & Bischoff, T. (2016). A Multibasin Residual-Mean Model for the Global Overturning Circulation. *Journal of Physical Oceanography*, *46*(9), 2583–2604. https://doi.org/10.1175/JPO-D-15-0204.1

Toggweiler, J. R., & Samuels, B. (1998). On the Ocean's Large-Scale Circulation near the Limit of No Vertical Mixing. *Journal of Physical Oceanography*, *28*(9), 1832–1852. https://doi.org/10.1175/1520-0485(1998)028

Weaver, A. J., Sedláček, J., Eby, M., Alexander, K., Crespin, E., Fichefet, T., Philippon-Berthier, G., Joos, F., Kawamiy, M., Matsumoto, K., Steinacher, M., Tachiiri, K., Tokos, K., Yoshimori, M., & Zickfeld, K. (2012). Stability of the Atlantic meridional overturning circulation: A model intercomparison. *Geophysical Research Letters*, *39*(20), 20709. https://doi.org/10.1029/2012GL053763

Weijer, W., Cheng, W., Drijfhout, S. S., Fedorov, A. v., Hu, A., Jackson, L. C., Liu, W., McDonagh, E. L., Mecking, J. v., & Zhang, J. (2019). Stability of the Atlantic Meridional Overturning Circulation: A Review and Synthesis. *Journal of Geophysical Research: Oceans*, *124*(8), 5336–5375. https://doi.org/10.1029/2019JC015083

Weijer, W., Cheng, W., Garuba, O. A., Hu, A., & Nadiga, B. T. (2020). CMIP6 Models Predict Significant 21st Century Decline of the Atlantic Meridional Overturning Circulation. *Geophysical Research Letters*, *47*(12), e2019GL086075. https://doi.org/10.1029/2019GL086075

Winton, M., Anderson, W. G., Delworth, T. L., Griffies, S. M., Hurlin, W. J., & Rosati, A. (2014). Has coarse ocean resolution biased simulations of transient climate sensitivity? *Geophysical Research Letters*, *41*(23), 8522–8529. https://doi.org/10.1002/2014GL061523

References From the Supporting Information

Baker, J. A., Renshaw, R., Jackson, L. C., Dubois, C., Iovino, D., Zuo, H., Perez, R. C., Dong, S., Kersalé, M., Mayer, M., Mayer, J., Speich, S., and Lamont, T. (2022): Overturning and heat transport variations in the South Atlantic in an ocean reanalysis ensemble, State Planet Discuss. [preprint], https://doi.org/10.5194/sp-2022-8, in review.

Baker J., & Renshaw R. (2023). GloRanV14 ocean reanalysis MOC data [Data set]. Zenodo. https://doi.org/10.5281/zenodo.7649266

Moat, B. I., Frajka-Williams, E., Smeed, D. A., Rayner, D., Johns, W. E., Baringer, M. O., et al. (2022). Atlantic meridional overturning circulation observed by the RAPID-MOCHA-WBTS (RAPID-Meridional Overturning Circulation and Heatflux Array-Western Boundary Time Series) array at 26N from 2004 to 2020 (v2020.2). [Dataset]. British Oceanographic Data Centre, Natural Environment Research Council. https://doi.org/10.5285/e91b10af-6f0a-7fa7-e053-6c86abc05a09

Aldama-Campino, A., Fransner, F., Ödalen, M., Groeskamp, S., Yool, A., Döös, K., & Nycander, J. (2020). Meridional Ocean Carbon Transport. *Global Biogeochemical Cycles*, *34*(9), e2019GB006336. https://doi.org/10.1029/2019GB006336

Baker, J. A., Watson, A. J., & Vallis, G. K. (2020). Meridional overturning circulation in a multibasin model. Part i: Dependence on southern ocean buoyancy forcing. *Journal of Physical Oceanography*, *50*(5), 1159–1178. https://doi.org/10.1175/JPO-D-19-0135.1

Baker, J. A., Watson, A. J., & Vallis, G. K. (2021). Meridional Overturning Circulation in a Multibasin Model. Part II: Sensitivity to Diffusivity and Wind in Warm and Cool Climates. *Journal of Physical Oceanography*, *51*(6), 1813–1828. https://doi.org/10.1175/JPO-D-20-0121.1

Bellomo, K., Angeloni, M., Corti, S., & von Hardenberg, J. (2021). Future climate change shaped by inter-model differences in Atlantic meridional overturning circulation response. *Nature Communications 2021 12:1*, *12*(1), 1–10. https://doi.org/10.1038/s41467-021-24015-w

Bonan, D. B., Thompson, A. F., Newsom, E. R., Sun, S., & Rugenstein, M. (2022). Transient and Equilibrium Responses of the Atlantic Overturning Circulation to Warming in Coupled Climate Models: The Role of Temperature and Salinity. *Journal of Climate*, *35*(15), 5173–5193. https://doi.org/10.1175/jcli-d-21-0912.1

Buckley, M. W., & Marshall, J. (2016). Observations, inferences, and mechanisms of the Atlantic Meridional Overturning Circulation: A review. *Reviews of Geophysics*, *54*(1), 5–63. https://doi.org/10.1002/2015RG000493

Cessi, P. (2019). The Global Overturning Circulation. *Https://Doi.Org/10.1146/Annurev-Marine-010318-095241*, *11*, 249–270. https://doi.org/10.1146/ANNUREV-MARINE-010318-095241

578 Chang, C.-Y., & Jansen, M. F. (2022). The time-dependent response of a two-basin ocean to a sudden
579 surface temperature change. *Journal of Climate*, 1–34. https://doi.org/10.1175/jcli-d-21-0821.1

580 Cheng, W., Chiang, J. C. H., & Zhang, D. (2013). Atlantic Meridional Overturning Circulation (AMOC)
581 in CMIP5 Models: RCP and Historical Simulations. *Journal of Climate*, *26*(18), 7187–7197.
582 https://doi.org/10.1175/JCLI-D-12-00496.1

583 Deng, K., Azorin-Molina, C., Yang, S., Hu, C., Zhang, G., Minola, L., & Chen, D. (2022). Changes of
584 Southern Hemisphere westerlies in the future warming climate. *Atmospheric Research*, *270*,
585 106040. https://doi.org/10.1016/J.ATMOSRES.2022.106040

586 Dixon, K. W., Delworth, T. L., Spelman, M. J., & Stouffer, R. J. (1999). The influence of transient
587 surface fluxes on North Atlantic overturning in a coupled GCM Climate Change Experiment.
588 *Geophysical Research Letters*, *26*(17), 2749–2752. https://doi.org/10.1029/1999GL900571

589 Eyring, V., Bony, S., Meehl, G. A., Senior, C. A., Stevens, B., Stouffer, R. J., & Taylor, K. E. (1937).
590 Overview of the Coupled Model Intercomparison Project Phase 6 (CMIP6) experimental design
591 and organization. *Geosci. Model Dev*, *9*. https://doi.org/10.5194/gmd-9-1937-2016

592 Ferrari, R., Jansen, M. F., Adkins, J. F., Burke, A., Stewart, A. L., & Thompson, A. F. (2014). Antarctic
593 sea ice control on ocean circulation in present and glacial climates. *Proceedings of the National*
594 *Academy of Sciences of the United States of America*, *111*(24), 8753–8758.
595 https://doi.org/10.1073/PNAS.1323922111/SUPPL_FILE/PNAS.201323922SI.PDF

596 Ferrari, R., Nadeau L-P, Marshall, D., Allison, L. C., & Johnson, H. L. (2017). A Model of the Ocean
597 Overturning Circulation with Two Closed Basins and a Reentrant Channel. *J. Phys. Oceanogr.*,
598 *47*, 2887–2906. https://doi.org/10.1175/JPO-D-16-0223.1

599 Forget, G., Campin, J. M., Heimbach, P., Hill, C. N., Ponte, R. M., & Wunsch, C. (2015). ECCO version
600 4: An integrated framework for non-linear inverse modeling and global ocean state estimation.
601 *Geoscientific Model Development*, *8*(10), 3071–3104. https://doi.org/10.5194/GMD-8-3071-
602 2015

603 Gregory, J. M., Dixon, K. W., Stouffer, R. J., Weaver, A. J., Driesschaert, E., Eby, M., Fichefet, T.,
604 Hasumi, H., Hu, A., Jungclaus, J. H., Kamenkovich, I. v, Levermann, A., Montoya, M., Murakami,
605 S., Nawrath, S., Oka, A., Sokolov, A. P., & Thorpe, R. B. (2005). *A model intercomparison of*
606 *changes in the Atlantic thermohaline circulation in response to increasing atmospheric*
607 *CO<subscr>2</subscr> concentration*. https://doi.org/10.1029/2005GL023209

608 Gregory, J. M., & Tailleux, R. (2011). Kinetic energy analysis of the response of the Atlantic
609 meridional overturning circulation to CO2-forced climate change. *Climate Dynamics*, *37*(5),
610 893–914. https://doi.org/10.1007/S00382-010-0847-6/FIGURES/11

611 Griffies, S. M., Danabasoglu, G., Durack, P. J., Adcroft, A. J., Balaji, V., Böning, C. W., Chassignet, E. P.,
612 Curchitser, E., Deshayes, J., Drange, H., Fox-Kemper, B., Gleckler, P. J., Gregory, J. M., Haak, H.,
613 Hallberg, R. W., Heimbach, P., Hewitt, H. T., Holland, D. M., Ilyina, T., … Yeager, S. G. (2016).
614 OMIP contribution to CMIP6: Experimental and diagnostic protocol for the physical component
615 of the Ocean Model Intercomparison Project. *Geoscientific Model Development*, *9*(9), 3231–
616 3296. https://doi.org/10.5194/GMD-9-3231-2016

617 Hallberg, R., & Gnanadesikan, A. (2006). The Role of Eddies in Determining the Structure and
618 Response of the Wind-Driven Southern Hemisphere Overturning: Results from the Modeling

Eddies in the Southern Ocean (MESO) Project. *Journal of Physical Oceanography*, *36*(12), 2232–2252. https://doi.org/10.1175/JPO2980.1

Heuzé, C. (2021). Antarctic Bottom Water and North Atlantic Deep Water in CMIP6 models. *Ocean Science*, *17*(1), 59–90. https://doi.org/10.5194/os-17-59-2021

Hu, A., van Roekel, L., Weijer, W., Garuba, O. A., Cheng, W., & Nadiga, B. T. (2020). Role of AMOC in Transient Climate Response to Greenhouse Gas Forcing in Two Coupled Models. *Journal of Climate*, *33*(14), 5845–5859. https://doi.org/10.1175/JCLI-D-19-1027.1

Jackson, L. C., Roberts, M. J., Hewitt, H. T., Iovino, D., Koenigk, T., Meccia, V. L., Roberts, C. D., Ruprich-Robert, Y., & Wood, R. A. (2020). Impact of ocean resolution and mean state on the rate of AMOC weakening. *Climate Dynamics*, *55*(7–8), 1711–1732. https://doi.org/10.1007/s00382-020-05345-9

Jones, C. S., & Cessi, P. (2016). Interbasin Transport of the Meridional Overturning Circulation. *Journal of Physical Oceanography*, *46*(4), 1157–1169. https://doi.org/10.1175/JPO-D-15-0197.1

Lee, S. K., Lumpkin, R., Baringer, M. O., Meinen, C. S., Goes, M., Dong, S., Lopez, H., & Yeager, S. G. (2019). Global Meridional Overturning Circulation Inferred From a Data-Constrained Ocean & Sea-Ice Model. *Geophysical Research Letters*, *46*(3), 1521–1530. https://doi.org/10.1029/2018GL080940

Levermann, A., Mignot, J., Nawrath, S., & Rahmstorf, S. (2007). *The Role of Northern Sea Ice Cover for the Weakening of the Thermohaline Circulation under Global Warming*. https://doi.org/10.1175/JCLI4232.1

Liu, W., Fedorov, A. v., Xie, S. P., & Hu, S. (2020). Climate impacts of a weakened Atlantic meridional overturning circulation in a warming climate. *Science Advances*, *6*(26). https://doi.org/10.1126/SCIADV.AAZ4876/SUPPL_FILE/AAZ4876_SM.PDF

Lumpkin, R., & Speer, K. (2007). Global Ocean Meridional Overturning. *Journal of Physical Oceanography*, *37*(10), 2550–2562. https://doi.org/10.1175/JPO3130.1

Menary, M. B., Hodson, D. L. R., Robson, J. I., Sutton, R. T., Wood, R. A., & Hunt, J. A. (2015). Exploring the impact of CMIP5 model biases on the simulation of North Atlantic decadal variability. *Geophysical Research Letters*, *42*(14), 5926–5934. https://doi.org/10.1002/2015GL064360

Munk, W., & Wunsch, C. (1998). Abyssal recipes II: energetics of tidal and wind mixing. *Deep Sea Research Part I: Oceanographic Research Papers*, *45*(12), 1977–2010. https://doi.org/10.1016/S0967-0637(98)00070-3

Nadeau, L. P., & Jansen, M. F. (2020). Overturning Circulation Pathways in a Two-Basin Ocean Model. *Journal of Physical Oceanography*, *50*(8), 2105–2122. https://doi.org/10.1175/JPO-D-20-0034.1

Newsom, E. R., & Thompson, A. F. (2018). Reassessing the Role of the Indo-Pacific in the Ocean's Global Overturning Circulation. *Geophysical Research Letters*, *45*(22), 12,422-12,431. https://doi.org/10.1029/2018GL080350

O'Neill, B. C., Tebaldi, C., van Vuuren, D. P., Eyring, V., Friedlingstein, P., Hurtt, G., Knutti, R., Kriegler, E., Lamarque, J.-F., Lowe, J., Meehl, G. A., Moss, R., Riahi, K., & Sanderson, B. M. (2016). The

Scenario Model Intercomparison Project (ScenarioMIP) for CMIP6. *Geosci. Model Dev*, *9*, 3461–3482. https://doi.org/10.5194/gmd-9-3461-2016

Rahmstorf, S. (2015). Exceptional twentieth-century slowdown in Atlantic Ocean overturning circulation. *Nat. Clim. Chang.*, *5*(5), 475–480. https://doi.org/10.1038/nclimate2554

Riahi, K., van Vuuren, D. P., Kriegler, E., Edmonds, J., O'Neill, B. C., Fujimori, S., Bauer, N., Calvin, K., Dellink, R., Fricko, O., Lutz, W., Popp, A., Cuaresma, J. C., KC, S., Leimbach, M., Jiang, L., Kram, T., Rao, S., Emmerling, J., … Tavoni, M. (2017). The Shared Socioeconomic Pathways and their energy, land use, and greenhouse gas emissions implications: An overview. *Global Environmental Change*, *42*, 153–168. https://doi.org/10.1016/J.GLOENVCHA.2016.05.009

Rugenstein, M. A. A., Winton, M., Stouffer, R. J., Griffies, S. M., & Hallberg, R. (2013). Northern High-Latitude Heat Budget Decomposition and Transient Warming. *Journal of Climate*, *26*(2), 609–621. https://doi.org/10.1175/JCLI-D-11-00695.1

Schmittner, A., Latif, M., & Schneider, B. (2005). Model projections of the North Atlantic thermohaline circulation for the 21st century assessed by observations. *Geophysical Research Letters*, *32*(23), 1–4. https://doi.org/10.1029/2005GL024368

Stouffer, R. J., Yin, J., Gregory, J. M., Dixon, K. W., Spelman, M. J., Hurlin, W., Weaver, A. J., Eby, M., Flato, G. M., Hasumi, H., Hu, A., Jungclaus, J. H., Kamenkovich, I. v., Levermann, A., Montoya, M., Murakami, S., Nawrath, S., Oka, A., Peltier, W. R., … Weber, S. L. (2006). Investigating the Causes of the Response of the Thermohaline Circulation to Past and Future Climate Changes. *Journal of Climate*, *19*(8), 1365–1387. https://doi.org/10.1175/JCLI3689.1

Sun, S., Thompson, A. F., & Eisenman, I. (2020). Transient Overturning Compensation between Atlantic and Indo-Pacific Basins. *Journal of Physical Oceanography*, *50*(8), 2151–2172. https://doi.org/10.1175/JPO-D-20-0060.1

Sun, S., Thompson, A. F., Xie, S. P., & Long, S. M. (2022). Indo-Pacific Warming Induced by a Weakening of the Atlantic Meridional Overturning Circulation. *Journal of Climate*, *35*(2), 815–832. https://doi.org/10.1175/JCLI-D-21-0346.1

Talley, L. D. (2013). Closure of the global overturning circulation through the Indian, Pacific, and southern oceans. *Oceanography*, *26*(1), 80–97. https://doi.org/10.5670/OCEANOG.2013.07

Thompson, A. F., Stewart, A. L., & Bischoff, T. (2016). A Multibasin Residual-Mean Model for the Global Overturning Circulation. *Journal of Physical Oceanography*, *46*(9), 2583–2604. https://doi.org/10.1175/JPO-D-15-0204.1

Toggweiler, J. R., & Samuels, B. (1998). On the Ocean's Large-Scale Circulation near the Limit of No Vertical Mixing. *Journal of Physical Oceanography*, *28*(9), 1832–1852. https://doi.org/10.1175/1520-0485(1998)028

Weaver, A. J., Sedláček, J., Eby, M., Alexander, K., Crespin, E., Fichefet, T., Philippon-Berthier, G., Joos, F., Kawamiy, M., Matsumoto, K., Steinacher, M., Tachiiri, K., Tokos, K., Yoshimori, M., & Zickfeld, K. (2012). Stability of the Atlantic meridional overturning circulation: A model intercomparison. *Geophysical Research Letters*, *39*(20), 20709. https://doi.org/10.1029/2012GL053763

Weijer, W., Cheng, W., Drijfhout, S. S., Fedorov, A. v., Hu, A., Jackson, L. C., Liu, W., McDonagh, E. L., Mecking, J. v., & Zhang, J. (2019). Stability of the Atlantic Meridional Overturning Circulation: A

699 Review and Synthesis. *Journal of Geophysical Research: Oceans*, *124*(8), 5336–5375.
700 https://doi.org/10.1029/2019JC015083

701 Weijer, W., Cheng, W., Garuba, O. A., Hu, A., & Nadiga, B. T. (2020). CMIP6 Models Predict
702 Significant 21st Century Decline of the Atlantic Meridional Overturning Circulation. *Geophysical*
703 *Research Letters*, *47*(12), e2019GL086075. https://doi.org/10.1029/2019GL086075

704 Winton, M., Anderson, W. G., Delworth, T. L., Griffies, S. M., Hurlin, W. J., & Rosati, A. (2014). Has
705 coarse ocean resolution biased simulations of transient climate sensitivity? *Geophysical*
706 *Research Letters*, *41*(23), 8522–8529. https://doi.org/10.1002/2014GL061523

707

Geophysical Research Letters

Supporting Information for

Overturning Pathways Control AMOC Weakening in CMIP6 Models

Baker J.A.[1], Bell M.J. [1], Jackson L.J. [1], Renshaw R. [1], Vallis G.K. [2], Watson A.J. [2], Wood R.A. [1]

[1] Met Office, UK.

[2] University of Exeter, UK.

Correspondence to: Jonathan Baker (jonathan.baker@metoffice.gov.uk)

Contents of this file

Model	Modeling Center	Ensemble member	Reference
ACCESS-CM2*	CSIRO-ARCCSS	r1i1p1f1	Bi et al. (2020)
ACCESS-ESM1-5*	CSIRO	r1i1p1f1	Ziehn et al. (2017, 2020)
CAS-ESM2-0*	CAS	r1i1p1f1	Zhang et al. (2020)
CESM2	NCAR	r1i1p1f1	Danabasoglu et al. (2020)
CESM2-FV2	NCAR	r1i1p1f1	Danabasoglu et al. (2020)
CESM2-WACCM*	NCAR	r1i1p1f1	Danabasoglu et al. (2020)
CESM2-WACCM-FV2	NCAR	r1i1p1f1	Danabasoglu et al. (2020)
CIESM	Tsinghua University	r1i1p1f1	Lin et al. (2020)
CMCC-CM2-HR4*	CMCC	r1i1p1f1	Cherchi et al. (2019)
CMCC-CM2-SR5*	CMCC	r1i1p1f1	Cherchi et al. (2019)
CMCC-ESM2	CMCC	r1i1p1f1	Lovato et al. (2022)
CNRM-CM6-1*	CNRM-CERFACS	r1i1p1f2	Voldoire et al. (2019)
CNRM-CM6-1-HR*	CNRM-CERFACS	r1i1p1f2	N/A
CNRM-ESM2-1*	CNRM-CERFACS	r1i1p1f2	Séférian et al. (2019)
CanESM5*	CCCma	r1i1p1f1	Swart et al. (2019)
E3SM-1-0	E3SM Project	r1i1p1f1	Golaz et al. (2019)
E3SM-1-1	E3SM Project	r1i1p1f1	Golaz et al. (2019)
E3SM-1-1-ECA	E3SM Project	r1i1p1f1	Golaz et al. (2019)
EC-Earth3	EC-Earth Consortium	r1i1p1f1	Wyser et al. (2020)
EC-Earth3-AerChem	EC-Earth Consortium	r1i1p1f1	Wyser et al. (2020)
EC-Earth3-CC	EC-Earth Consortium	r1i1p1f1	Wyser et al. (2020)
EC-Earth3-Veg	EC-Earth Consortium	r1i1p1f1	Wyser et al. (2020)
EC-Earth3-Veg-LR	EC-Earth Consortium	r1i1p1f1	Wyser et al. (2020)
FGOALS-f3-L*	CAS	r1i1p1f1	He et al. (2020)
FGOALS-g3*	CAS	r1i1p1f1	Li et al. (2020)
GFDL-CM4	NOAA	r1i1p1f1	Held et al., (2019)
GFDL-ESM4	NOAA	r1i1p1f1	Dunne et al. (2020)

GISS-E2-1-G-CC	NASA-GISS	r1i1p1f1	Kelley et al., (2020)
GISS-E2-1-G*	NASA-GISS	r1i1p1f2	Kelley et al., (2020)
HadGEM3-GC31-LL*	MOHC	r1i1p1f3	Kuhlbrodt et al. (2018)
HadGEM3-GC31-MM*	MOHC	r1i1p1f3	Andrews et al., (2020); Williams et al., (2018)
ICON-ESM-LR	MPI	r1i1p1f1	Jungclaus et al., (2022)
INM-CM4-8*	INM	r1i1p1f1	(Volodin et al. (2018)
INM-CM5-0*	INM	r1i1p1f1	Volodin & Gritsun (2018)
IPSL-CM6A-LR*	IPSL	r1i1p1f1	Boucher et al. (2020); Lurton et al. (2020)
IPSL-CM6A-LR-INCA	IPSL	r1i1p1f1	Boucher et al., (2020)
MIROC6*	JAMSTEC, NIES, AORI, U. of Tokyo	r1i1p1f1	Tatebe et al. (2019)
MPI-ESM-1-2-HAM	MPI	r1i1p1f1	Mauritsen et al. (2019)
MPI-ESM1-2-HR*	MPI	r1i1p1f1	Gutjahr et al. (2019); Müller et al. (2018)
MPI-ESM1-2-LR*	MPI	r1i1p1f1	Mauritsen et al. (2019)
MRI-ESM2-0*	MRI	r1i1p1f1	Yukimoto et al. (2019)
NorCPM1	NCC	r1i1p1f1	Bethke et al. (2021)
NorESM2-LM*	NCC	r1i1p1f1	Tjiputra et al. (2020)
NorESM2-MM*	NCC	r1i1p1f1	Tjiputra et al. (2020)
SAM0-UNICON	SNU	r1i1p1f1	Park et al. (2019)
UKESM1-0-LL*	MOHC	r1i1p1f2	Sellar et al. (2019)
UKESM1-1-LL	MOHC	r1i1p1f2	Sellar et al. (2019)

Table S1. List of the 49 CMIP6 models used in this study (i.e., the historical simulations that provide the overturning streamfunction). Models with a '*' superscript are used in our ssp585 experiment analysis.

	Observation-based estimates			
	GloRanV14 (2000-2021)	ECCOv4 (density space) (1992-2015)	Robust diagnostic simulation (Lee et al., 2019)	Inverse model estimate at 32°S (Lumpkin & Speer, 2007)
$AMOC_{max}$ (Sv)	18.9	18	25	18
AMOC_34.5°S (Sv)	15.6	14	16.9 (30°S)	12.4
$NADW\_wind_{total}$ (Sv)	7.6	14	-	11
$NADW\_IP_{diffu}$ (Sv)	8.1	0	~6.5	1.4
AMOC weakening based on emergent constraint (Sv) (2080-2100, ssp126 forcing)	6.0 (32%) (36% relative to RAPID AMOC)	3.0 (17%) (18% relative to RAPID AMOC)	5.4 (22%) (32% relative to RAPID AMOC)	3.5 (19%) (21% relative to RAPID AMOC)
AMOC weakening based on emergent constraint (Sv) (2080-2100, ssp585 forcing)	11.6 (61%) (67% relative to RAPID AMOC)	5.2 (29%) (31% relative to RAPID AMOC)	10.3 (41%) (61% relative to RAPID AMOC)	6.3 (35%) (37% relative to RAPID AMOC)

Table S2. Observation-based estimates of the AMOC strength, the overturning pathways and the AMOC weakening by 2080-2100 based on the CMIP6 Indo-Pacific diffusive pathway emergent constraint relationship under ssp126 and ssp585 forcing. The % weakening is shown relative to $AMOC_{max}$ in the observation-based estimate and relative to the time-mean RAPID/MOCHA (Rapid Climate Change-Meridional Overturning Circulation and Heatflux Array) AMOC estimate at 26.5°N of 16.9 Sv, averaged from April 2004 to September 2018 (Moat et al., 2022).

No	MOC Pathway	Abbreviation	Definition
(1)	Atlantic diffusive pathway	"NADW_At$_{diffu}$"	NADW pathway that upwells diffusively (or via eddy-induced circulations) in the Atlantic basin and returns to the North Atlantic at shallower depths without entering the Southern Ocean (SO).
(2)	Total Southern Ocean wind pathway	"NADW_wind$_{total}$" (4) + (5)	Total volume of the AMOC upwelled by the SO upper wind-driven cell that is approximately equal to the strength of the SO upper cell at 34.5°S.
(3)	Total Indo-Pacific pathway	"NADW_IP$_{total}$" (5) + (6)	NADW pathway that flows into the Indo-Pacific basin via the SO, upwells diffusively and returns at shallower depths to the Atlantic basin.
(4)	Atlantic wind pathway	"NADW_At$_{wind}$"	NADW pathway that flows out of the Atlantic basin into the global-integrated SO wind-driven upper cell (i.e., flows into the SO above "Z_(SO_upper_cell)" in Figure 1) where it upwells and returns directly to the Atlantic basin at shallower depths.
(5)	Indo-Pacific wind pathway	"NADW_IP$_{wind}$"	Component of the Indo-Pacific pathway that upwells diffusively in the Indo-Pacific basin and is then upwelled further by the SO wind-driven upper cell, before returning to the Atlantic basin.
(6)	Indo-Pacific diffusive pathway	"NADW_IP$_{diffu}$"	Component of the Indo-Pacific pathway that upwells diffusively in the Indo-Pacific basin and then returns directly to the Atlantic basin via zonal flows in the SO (i.e., it is not upwelled by the SO upper cell).
(7)	Lower Indo-Pacific pathway	"NADW_IP$_{lower}$"	NADW pathway that flows out of the Atlantic basin into the global-integrated SO lower cell (i.e., below "Z_(SO_upper_cell)" in Figure 1), and then into the Indo-Pacific basin.
(8)	Upper Indo-Pacific pathway	"NADW_IP$_{upper}$"	NADW pathway that flows southward into the global-integrated SO upper cell (i.e., above "Z_(SO_upper_cell)"), and then into the Indo-Pacific basin.

Table S3. Overturning pathway definitions

Name	Definition
AMOC$_{max}$	Maximum strength of the AMOC in the North Atlantic
Z_AMOC	Depth of AMOC in the South Atlantic at 34.5°S
Z_(SO upper cell)	Depth of globally-integrated Southern Ocean (SO) upper cell at 34.5°S
Cell overlap	Depth of the overlap between the AMOC and the globally-integrated Southern Ocean lower cell at 34.5°S i.e., "Z_AMOC" – "Z_(SO upper cell)"

Table S4. Definitions of key terms and abbreviations

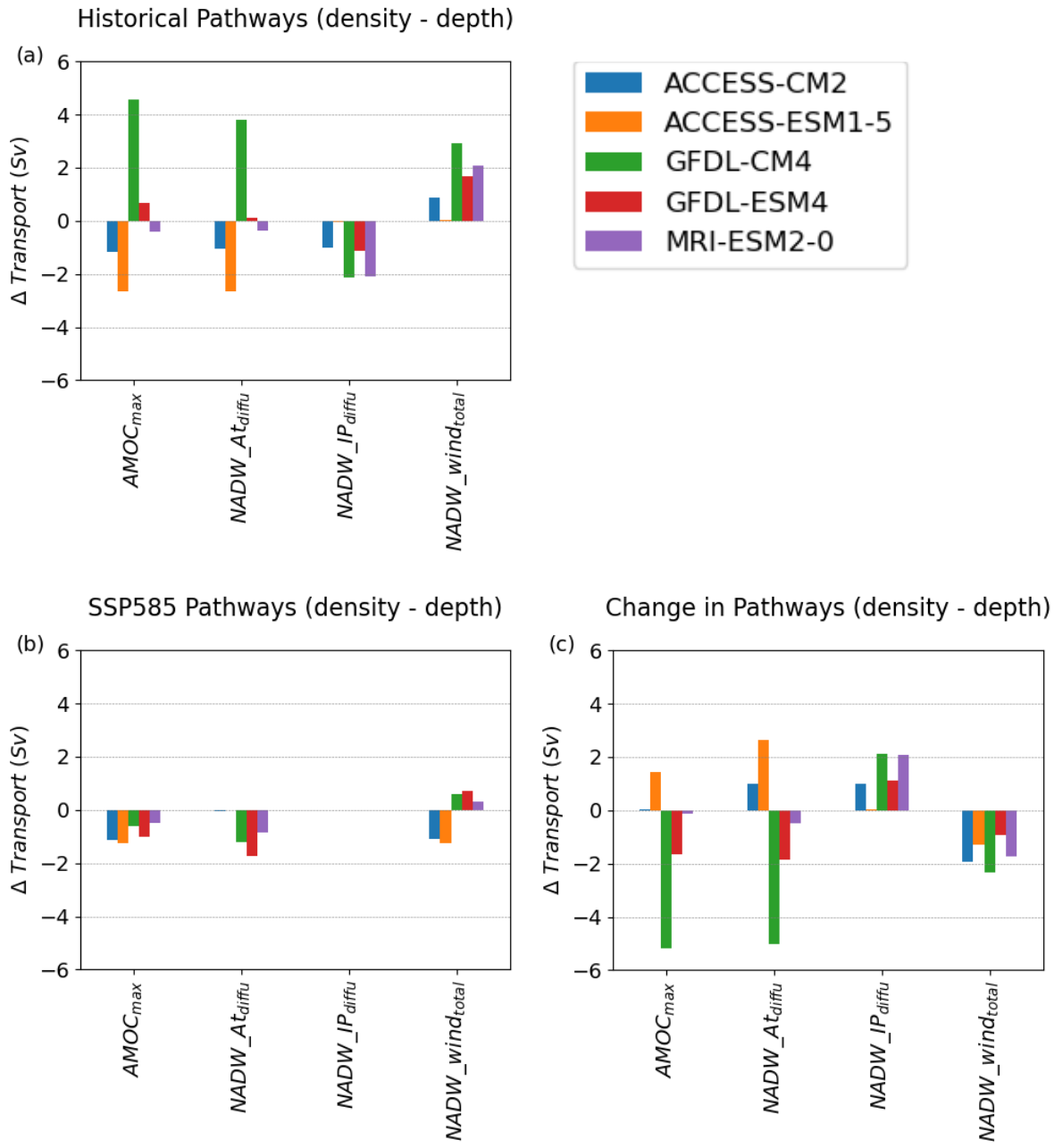

Figure S1. Difference between the AMOC strength and overturning pathways calculated in depth and density space in (a) the historical simulation (185-2014), (b) 2080-2100 of the ssp585 experiment and (c) the change between the historical simulation and 2080-2100 of ssp585.

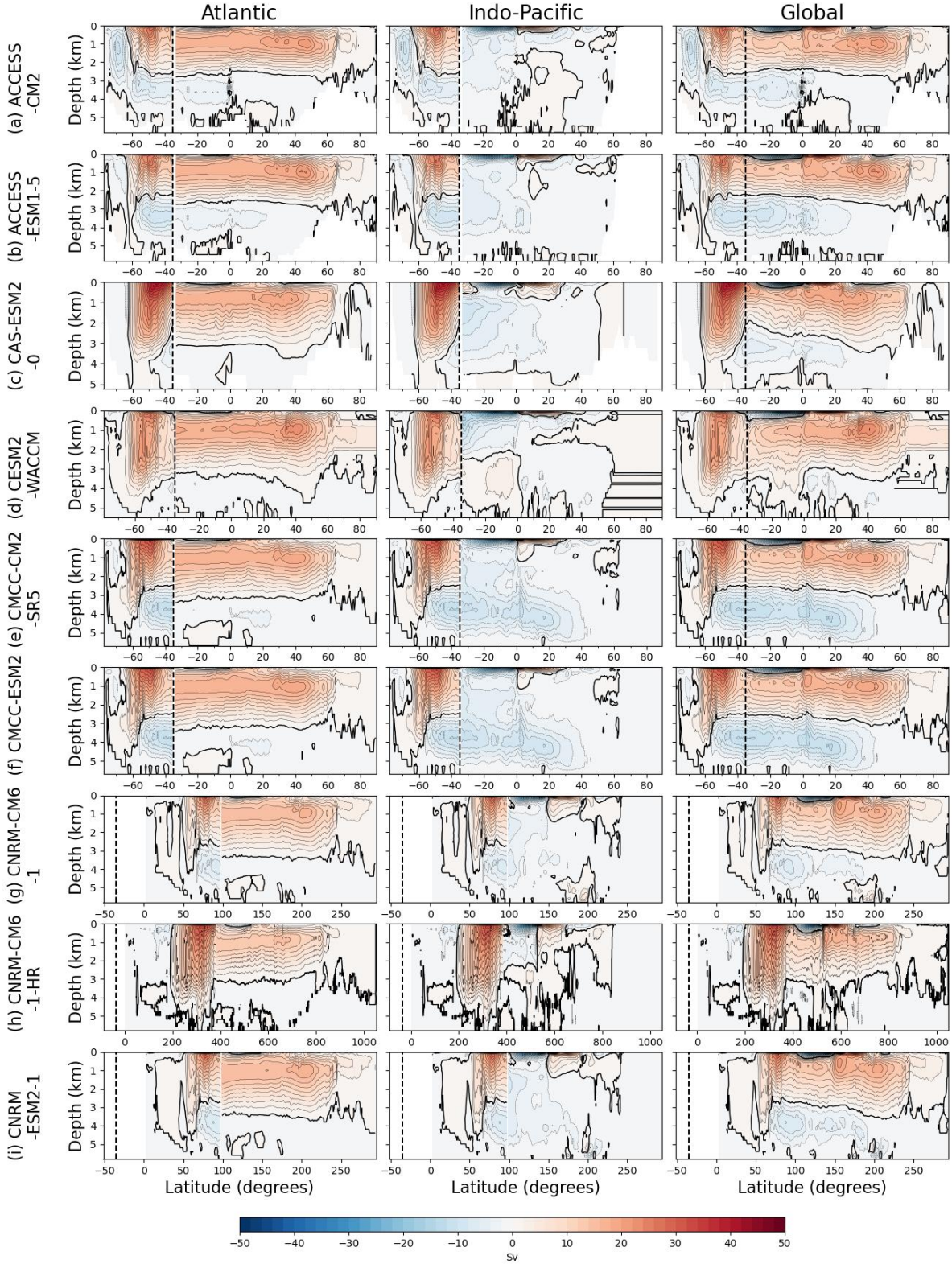
Atlantic
Indo-Pacific
Global
(a) ACCESS -CM2
(b) ACCESS -ESM1-5
(c) CAS-ESM2 -0
(d) CESM2 -WACCM
(e) CMCC-CM2 -SR5
(f) CMCC-ESM2
(g) CNRM-CM6 -1
(h) CNRM-CM6 -1-HR
(i) CNRM -ESM2-1
Depth (km)
Latitude (degrees)
Sv

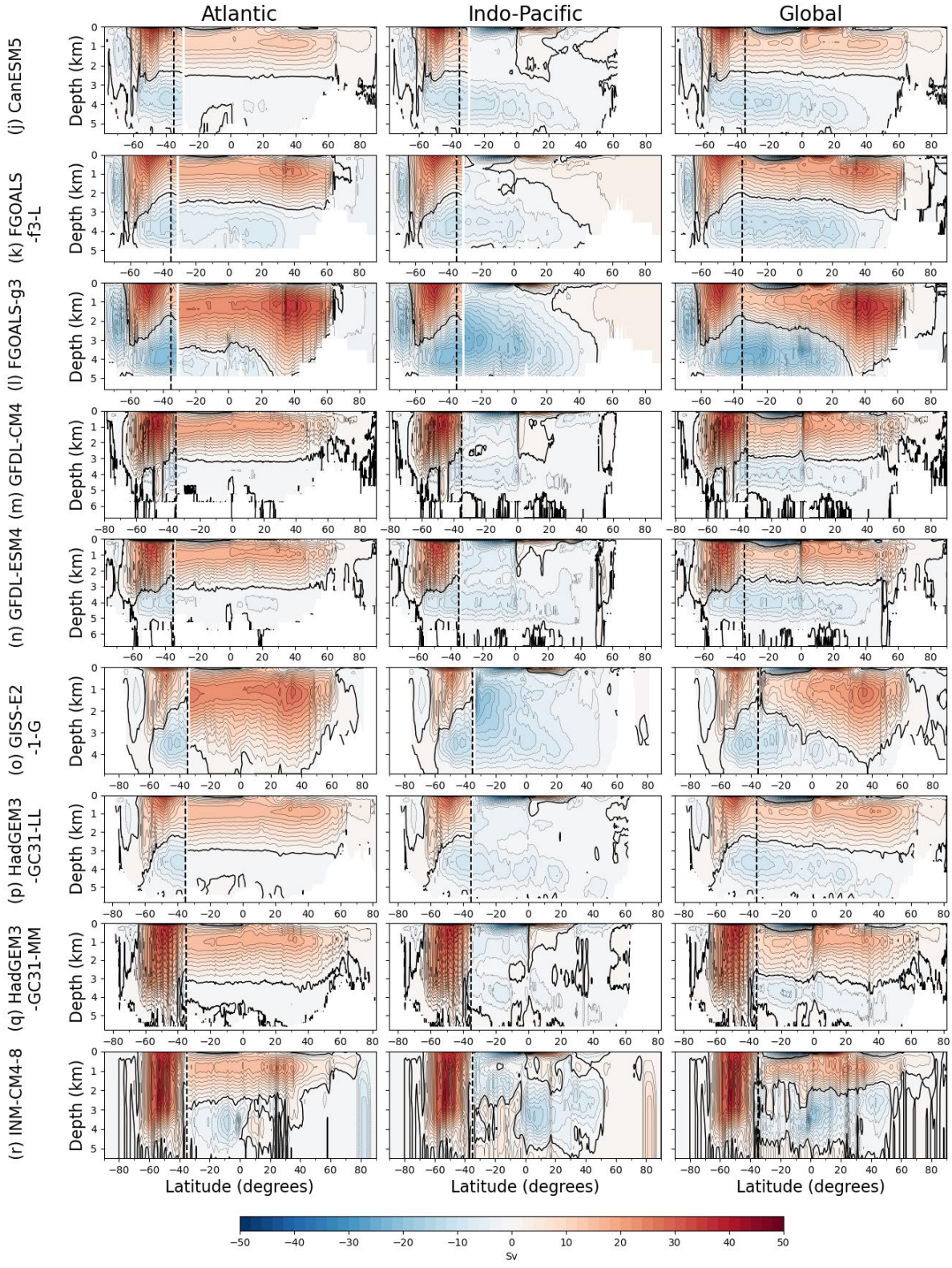
Atlantic
Indo-Pacific
Global
(j) CanESM5
(k) FGOALS -f3-L
(l) FGOALS-g3
(m) GFDL-CM4
(n) GFDL-ESM4
(o) GISS-E2 -1-G
(p) HadGEM3 -GC31-LL
(q) HadGEM3 -GC31-MM
(r) INM-CM4-8
Depth (km)
Latitude (degrees)
Sv

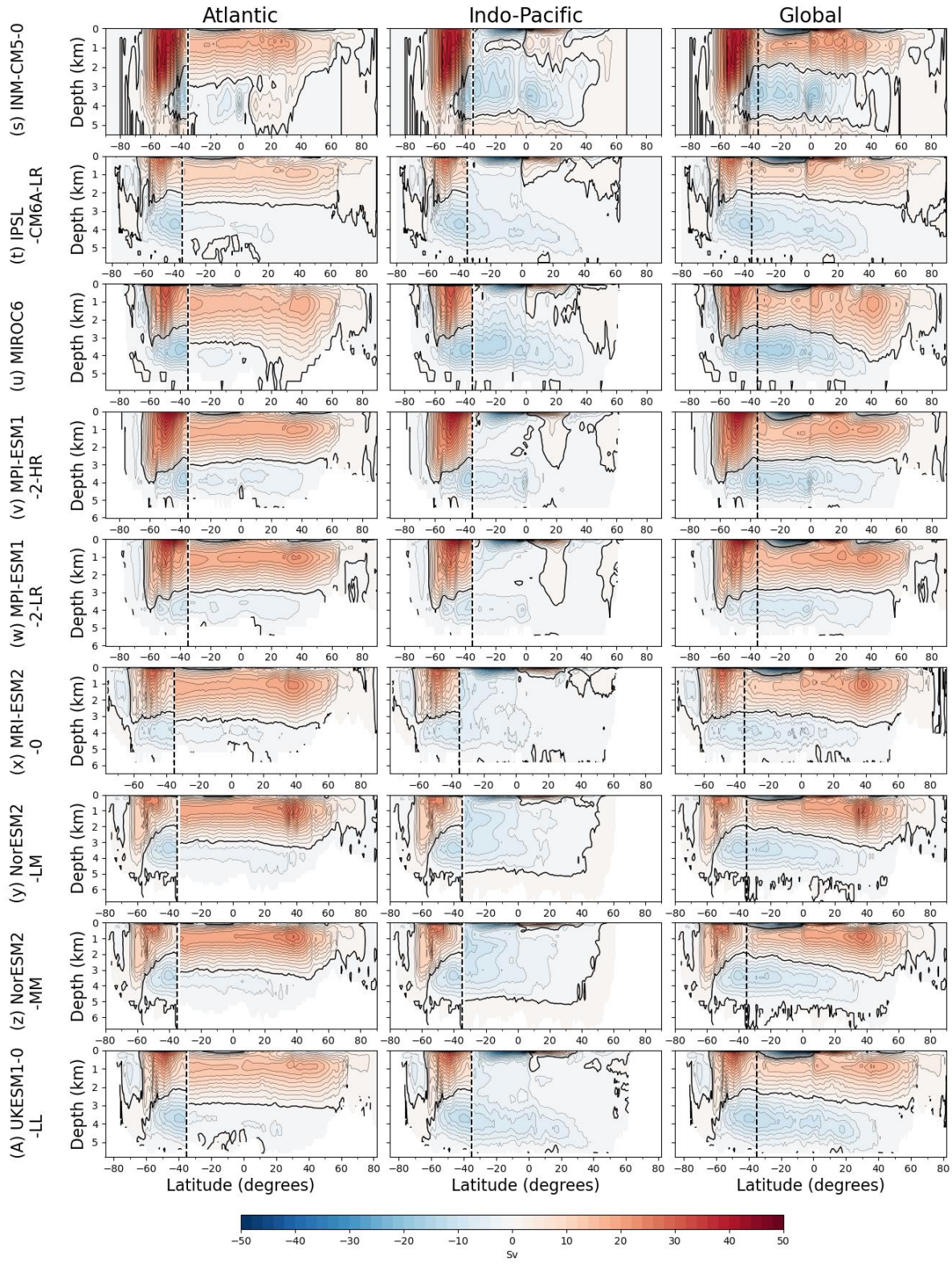

Figure S2. Overturning streamfunction (Sverdrups (Sv); 2 Sv contour interval) in depth space averaged over the 1850-2014 historical simulation in each model that has a ssp585 experiment. The zero-streamline contour is defined by the thick black line.

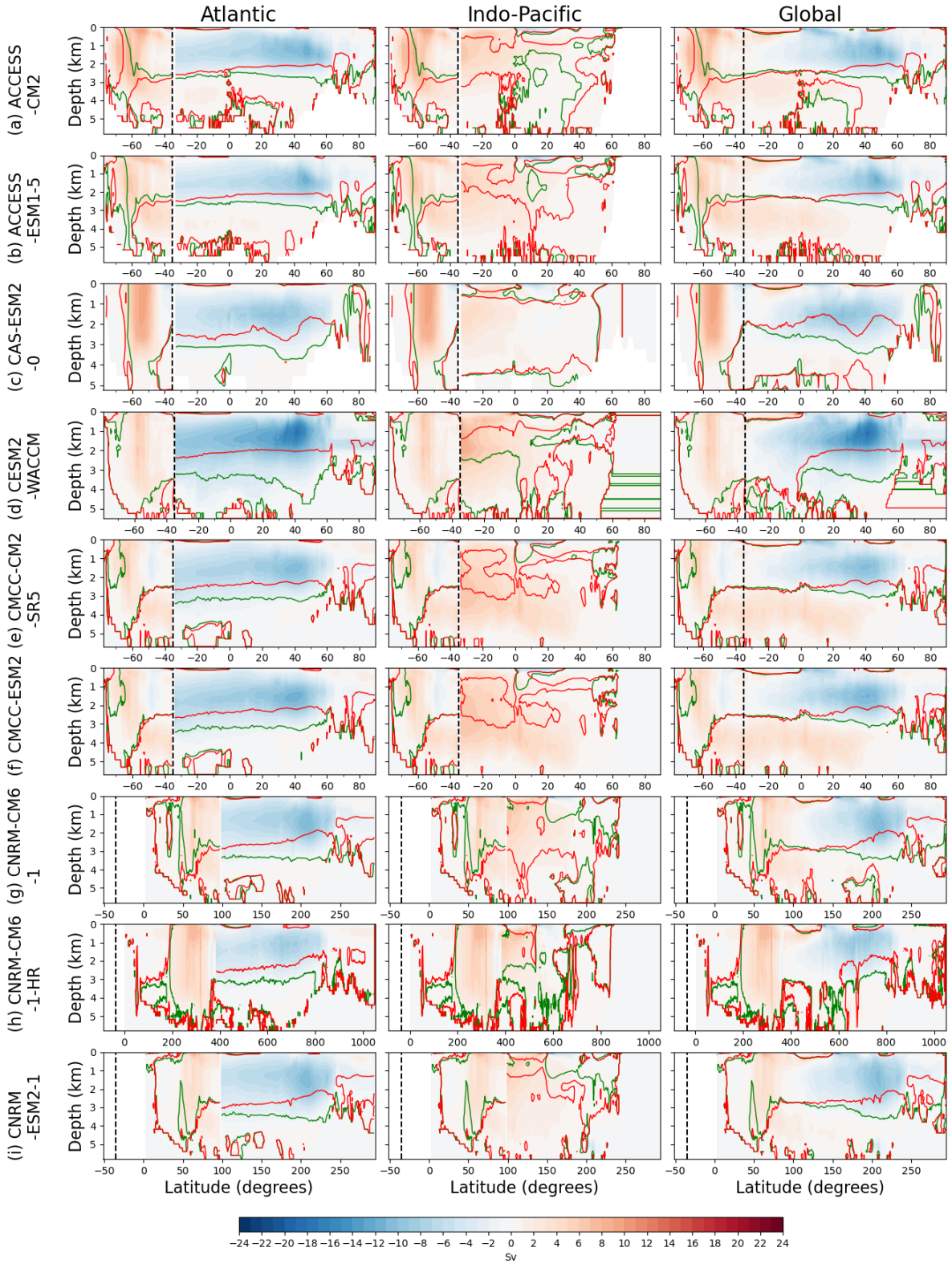
Atlantic
Indo-Pacific
Global
(a) ACCESS -CM2
(b) ACCESS -ESM1-5
(c) CAS-ESM2 -0
(d) CESM2 -WACCM
(e) CMCC-CM2 -SR5
(f) CMCC-ESM2
(g) CNRM-CM6 -1
(h) CNRM-CM6 -1-HR
(i) CNRM -ESM2-1
Depth (km)
Latitude (degrees)
Sv

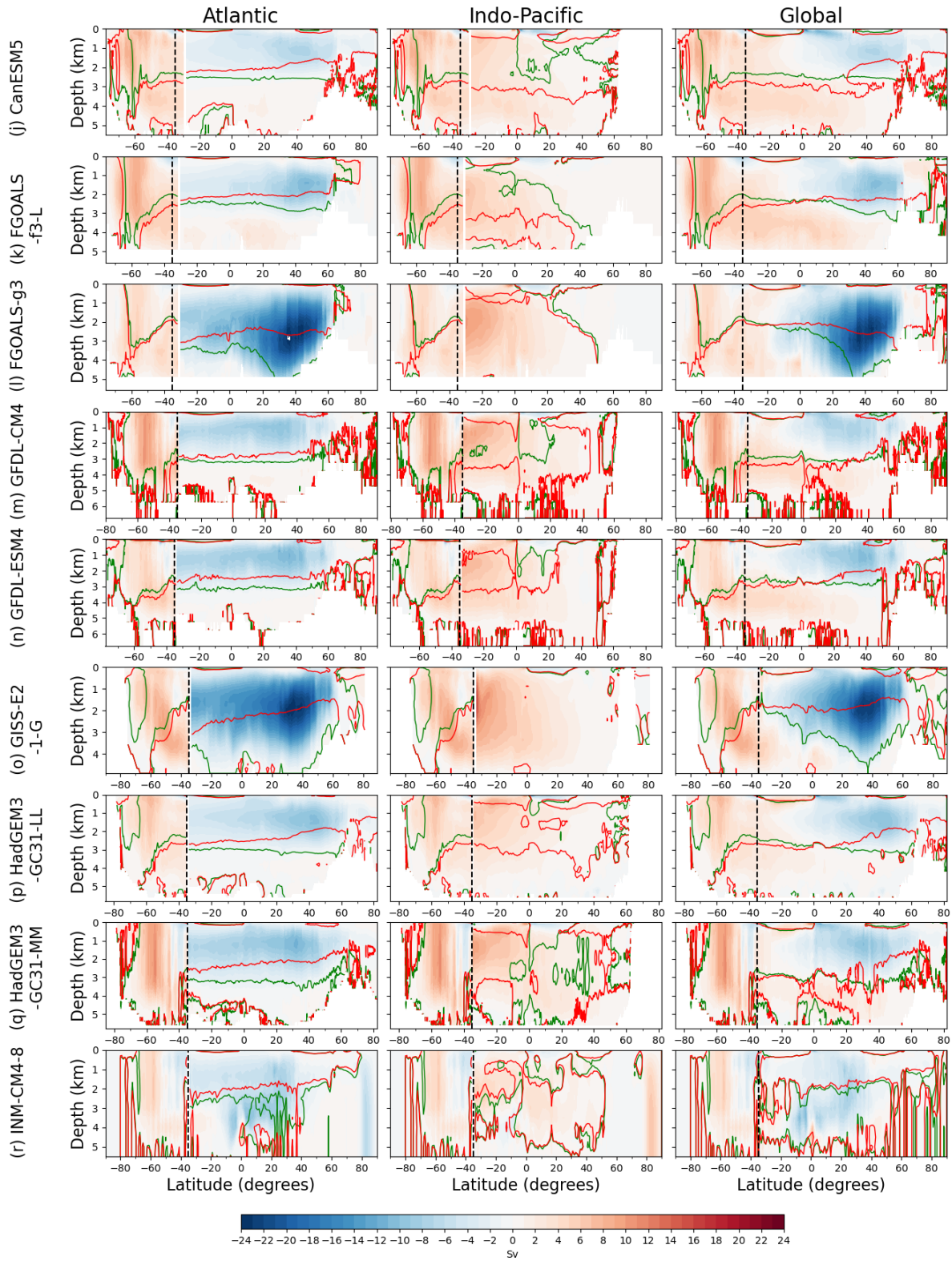
Atlantic
Indo-Pacific
Global
(j) CanESM5
(k) FGOALS -f3-L
(l) FGOALS-g3
(m) GFDL-CM4
(n) GFDL-ESM4
(o) GISS-E2 -1-G
(p) HadGEM3 -GC31-LL
(q) HadGEM3 -GC31-MM
(r) INM-CM4-8
Depth (km)
Latitude (degrees)
Sv

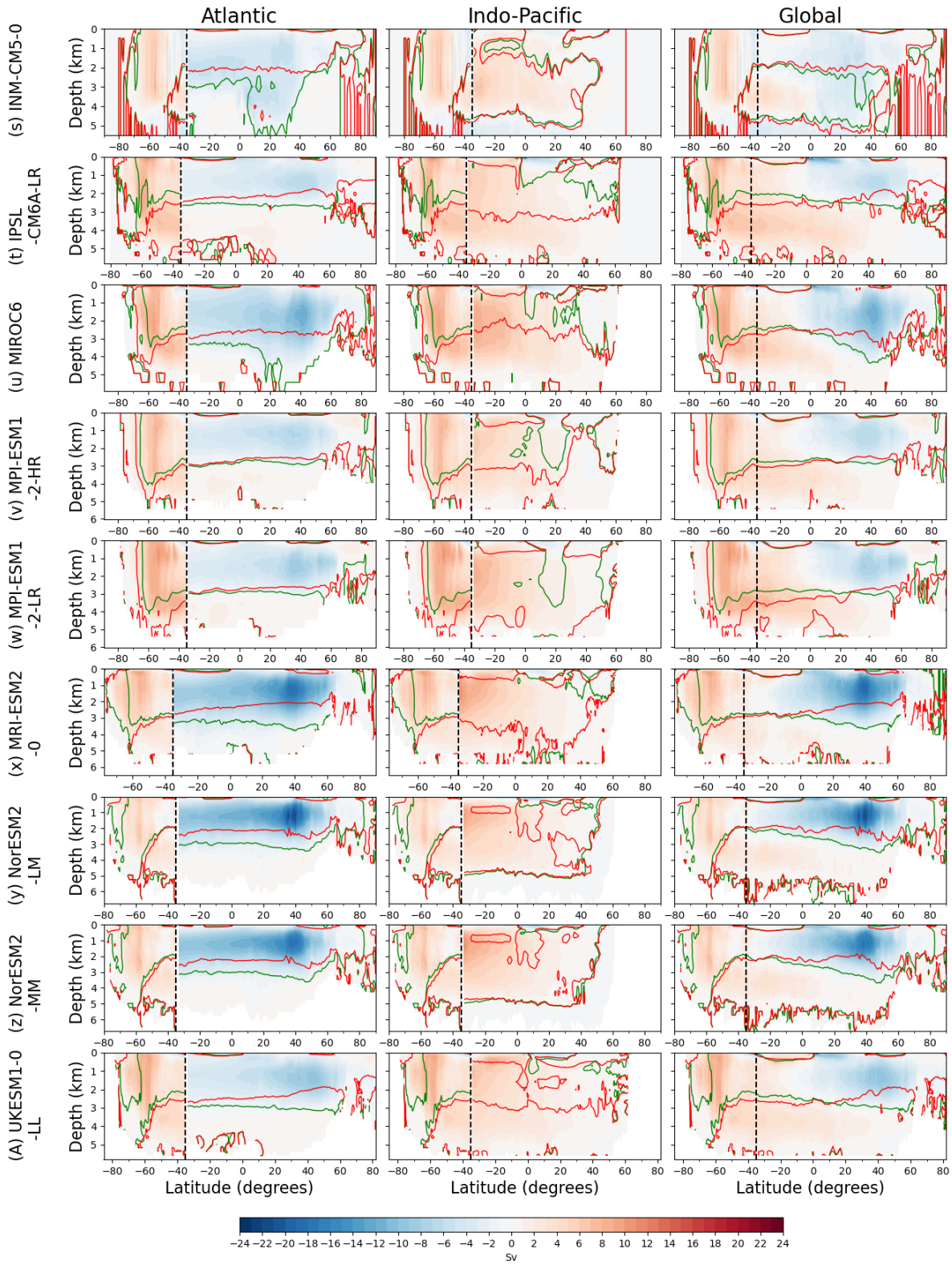

Figure S3. Changes in the overturning streamfunction (Sverdrups (Sv); 1 Sv contour interval) in depth space for the Atlantic, Indo-Pacific and global-average, calculated as the difference between the ssp585 experiment averaged over 2080-2100 and the historical experiment averaged over 1850-2014. The zero-streamline contour averaged over the historical simulation (green line) and from the 2080-2100 period of ssp585 (red line) are overlayed, so the location of the overturning cells and thus changes in the "cell overlap" can be inferred.

Equations used to separate the MOC pathways

We now define the equations linking the MOC pathways:

$$AMOC_{max} = NADW\_At_{diffu} + AMOC\,|_{\phi = 34.5°S} \quad \text{(eq. S1)}$$

$$NADW\_At_{diffu} = AMOC_{max} - AMOC\,|_{\phi = 34.5°S} \quad \text{(eq. S2)}$$

$$AMOC\,|_{\phi = 34.5°S} = NADW\_At_{wind} + NADW\_IP_{total}$$

$$= NADW\_wind_{total} + NADW\_IP_{diffu} \quad \text{(eq. S3)}$$

$$NADW\_IP_{wind} = NADW\_wind_{total} - NADW\_At_{wind} \quad \text{(eq. S4)}$$

$$NADW\_IP_{diffu} = NADW\_IP_{total} - NADW\_IP_{wind} \quad \text{(eq. S5)}$$

Modifications to the method of Baker et al. (2020,2021) *(BWV)*

We make several modifications to the *BWV* method to calculate the overturning pathways since we must account for overturning structures that were not present in the idealised model simulations of *BWV*. For example, a few of the CMIP6 models (e.g., CasESM) have localised clockwise meridional overturning cells at the southern boundary of the Indo-Pacific basin (see Figure S1). These cells export water southwards out of the Indo-Pacific basin, where, depending on their depth, they may upwell via the Southern Ocean (SO) upper cell. The magnitude of the Atlantic wind pathway or the Indo-Pacific wind pathway (and thus the total SO wind pathway) is therefore lower than that calculated using the original method due to upwelling of the NADW pathways by the SO upper cell decreasing (i.e., a reduced "total SO wind pathway").

In some models, the upper overturning streamfunction in the South Atlantic is not entirely connected to the NADW formation and subduction region in the North Atlantic. Instead, there is a "localised" circulation in both the North and South Atlantic, with no connection between these cells. Thus, when calculating the pathways of NADW, we reduce the pathway into the SO if a "localised" circulation is present in the South Atlantic. We determine the magnitude of this modified pathway by setting the pathway of NADW into the SO equal to the minimum AMOC strength located between 34.5°S and the latitude of the AMOC maximum in the North Atlantic. The remaining pathways are calculated as described previously, but using the modified pathway into the SO, $AMOC\,|_{\phi = 34.5°S}$. The Atlantic diffusive pathway calculated using the original method is increased by a magnitude equal to

the reduction in the pathway into the SO. Further modifications to the pathways are required if the "localised" South Atlantic MOC is upwelled by the SO upper cell as opposed to upwelling in the Indo-Pacific basin. We must then reduce the total SO wind pathway and increase the Indo-Pacific diffusive pathway by an equal magnitude. The proportion of the "localised" South Atlantic MOC that is upwelled in the Indo-Pacific basin is calculated from the change in the Indo-Pacific streamfunction at 34.5°S over the depth (or density range) of the "localised" cell. We note that while important, the differences when using this modified method do not change the qualitative results with similar correlations between the pathways and AMOC weakening.

Differences between depth and density space

We compare the overturning pathways calculated in depth and density space in five models, averaged over the historical simulation and over 2080-2100 in ssp585. Differences in the total SO wind and Indo-Pacific diffusive pathways are small relative to their absolute magnitudes (Figure S3a,b). In contrast, the Atlantic diffusive pathway has larger differences between these coordinate spaces in some models (Figure S3a,b), resulting in differences in AMOC strength and AMOC weakening (Figure S3c). Thus, the quantitative dependence of the AMOC weakening on both the historical AMOC strength and historical overturning pathways would change in density space. However, we expect our qualitative findings to be applicable in density space because the Indo-Pacific diffusive pathway is not significantly affected. The historical magnitude of this pathway is only slightly smaller in density space in most models. Thus, while the correlation between the Indo-Pacific diffusive pathway and AMOC weakening may differ in density space, it is likely be similar.

References

Andrews, M. B., Ridley, J. K., Wood, R. A., Andrews, T., Blockley, E. W., Booth, B., Burke, E., Dittus, A. J., Florek, P., Gray, L. J., Haddad, S., Hardiman, S. C., Hermanson, L., Hodson, D., Hogan, E., Jones, G. S., Knight, J. R., Kuhlbrodt, T., Misios, S., … Sutton, R. T. (2020). Historical Simulations With HadGEM3-GC3.1 for CMIP6. *Journal of Advances in Modeling Earth Systems*, *12*(6), e2019MS001995. https://doi.org/10.1029/2019MS001995

Bethke, I., Wang, Y., Counillon, F., Keenlyside, N., Kimmritz, M., Fransner, F., Samuelsen, A., Langehaug, H., Svendsen, L., Chiu, P. G., Passos, L., Bentsen, M., Guo, C., Gupta, A., Tjiputra, J., Kirkeväg, A., Olivié, Di., Seland, Ø., Solsvik Vägane, J., … Eldevik, T. (2021). NorCPM1 and its

contribution to CMIP6 DCPP. *Geoscientific Model Development*, *14*(11), 7073–7116. https://doi.org/10.5194/GMD-14-7073-2021

Bi, D., Dix, M., Marsland, S., O'farrell, S., Sullivan, A., Bodman, R., Law, R., Harman, I., Srbinovsky, J., Rashid, H. A., Dobrohotoff, P., Mackallah, C., Yan, H., Hirst, A., Savita, A., Boeira Dias, F., Woodhouse, M., Fiedler, R., & Heerdegen, A. (2020). Configuration and spin-up of ACCESS-CM2, the new generation Australian Community Climate and Earth System Simulator Coupled Model. *Journal of Southern Hemisphere Earth Systems Science*, *70*(1), 225–251. https://doi.org/10.1071/ES19040

Boucher, O., Servonnat, J., Albright, A. L., Aumont, O., Balkanski, Y., Bastrikov, V., Bekki, S., Bonnet, R., Bony, S., Bopp, L., Braconnot, P., Brockmann, P., Cadule, P., Caubel, A., Cheruy, F., Codron, F., Cozic, A., Cugnet, D., D'Andrea, F., … Vuichard, N. (2020). Presentation and Evaluation of the IPSL-CM6A-LR Climate Model. *Journal of Advances in Modeling Earth Systems*, *12*(7). https://doi.org/10.1029/2019MS002010

Cherchi, A., Fogli, P. G., Lovato, T., Peano, D., Iovino, D., Gualdi, S., Masina, S., Scoccimarro, E., Materia, S., Bellucci, A., & Navarra, A. (2019). Global Mean Climate and Main Patterns of Variability in the CMCC-CM2 Coupled Model. *Journal of Advances in Modeling Earth Systems*, *11*(1), 185–209. https://doi.org/10.1029/2018MS001369

Danabasoglu, G., Lamarque, J. F., Bacmeister, J., Bailey, D. A., DuVivier, A. K., Edwards, J., Emmons, L. K., Fasullo, J., Garcia, R., Gettelman, A., Hannay, C., Holland, M. M., Large, W. G., Lauritzen, P. H., Lawrence, D. M., Lenaerts, J. T. M., Lindsay, K., Lipscomb, W. H., Mills, M. J., … Strand, W. G. (2020). The Community Earth System Model Version 2 (CESM2). *Journal of Advances in Modeling Earth Systems*, *12*(2), e2019MS001916. https://doi.org/10.1029/2019MS001916

Dunne, J. P., Horowitz, L. W., Adcroft, A. J., Ginoux, P., Held, I. M., John, J. G., Krasting, J. P., Malyshev, S., Naik, V., Paulot, F., Shevliakova, E., Stock, C. A., Zadeh, N., Balaji, V., Blanton, C., Dunne, K. A., Dupuis, C., Durachta, J., Dussin, R., … Zhao, M. (2020). The GFDL Earth System Model Version 4.1 (GFDL-ESM 4.1): Overall Coupled Model Description and Simulation Characteristics. *Journal of Advances in Modeling Earth Systems*, *12*(11), e2019MS002015. https://doi.org/10.1029/2019MS002015

Golaz, J. C., Caldwell, P. M., van Roekel, L. P., Petersen, M. R., Tang, Q., Wolfe, J. D., Abeshu, G., Anantharaj, V., Asay-Davis, X. S., Bader, D. C., Baldwin, S. A., Bisht, G., Bogenschutz, P. A., Branstetter, M., Brunke, M. A., Brus, S. R., Burrows, S. M., Cameron-Smith, P. J., Donahue, A. S., … Zhu, Q. (2019). The DOE E3SM Coupled Model Version 1: Overview and Evaluation at Standard Resolution. *Journal of Advances in Modeling Earth Systems*, *11*(7), 2089–2129. https://doi.org/10.1029/2018MS001603

Gutjahr, O., Putrasahan, D., Lohmann, K., Jungclaus, J. H., von Storch, J. S., Brüggemann, N., Haak, H., & Stössel, A. (2019). Max Planck Institute Earth System Model (MPI-ESM1.2) for the High-Resolution Model Intercomparison Project (HighResMIP). *Geoscientific Model Development*, *12*(7), 3241–3281. https://doi.org/10.5194/GMD-12-3241-2019

He, B., Yu, Y., Bao, Q., Lin, P., Liu, H., Li, J., Wang, L., Liu, Y., Wu, G., Chen, K., Guo, Y., Zhao, S., Zhang, X., Song, M., Xie, J., Bian, H. E., Yongqiang, Y. U., Qing, B., Pengfei, L., … Jinbo, X. (2020). CAS FGOALS-f3-L model dataset descriptions for CMIP6 DECK experiments. *New Pub: KeAi*, 582–588. https://doi.org/10.1080/16742834.2020.1778419

Held, I. M., Guo, H., Adcroft, A., Dunne, J. P., Horowitz, L. W., Krasting, J., Shevliakova, E., Winton, M., Zhao, M., Bushuk, M., Wittenberg, A. T., Wyman, B., Xiang, B., Zhang, R., Anderson, W., Balaji, V., Donner, L., Dunne, K., Durachta, J., … Zadeh, N. (2019). Structure and Performance of GFDL's CM4.0 Climate Model. *Journal of Advances in Modeling Earth Systems*, *11*(11), 3691–3727. https://doi.org/10.1029/2019MS001829

Jungclaus, J. H., Lorenz, S. J., Schmidt, H., Brovkin, V., Brüggemann, N., Chegini, F., Crüger, T., De-Vrese, P., Gayler, V., Giorgetta, M. A., Gutjahr, O., Haak, H., Hagemann, S., Hanke, M., Ilyina, T., Korn, P., Kröger, J., Linardakis, L., Mehlmann, C., … Claussen, M. (2022). The ICON Earth System Model Version 1.0. *Journal of Advances in Modeling Earth Systems*, *14*(4), e2021MS002813. https://doi.org/10.1029/2021MS002813

Kelley, M., Schmidt, G. A., Nazarenko, L. S., Bauer, S. E., Ruedy, R., Russell, G. L., Ackerman, A. S., Aleinov, I., Bauer, M., Bleck, R., Canuto, V., Cesana, G., Cheng, Y., Clune, T. L., Cook, B. I., Cruz, C. A., del Genio, A. D., Elsaesser, G. S., Faluvegi, G., … Yao, M. S. (2020). GISS-E2.1: Configurations and Climatology. *Journal of Advances in Modeling Earth Systems*, *12*(8), e2019MS002025. https://doi.org/10.1029/2019MS002025

Kuhlbrodt, T., Jones, C. G., Sellar, A., Storkey, D., Blockley, E., Stringer, M., Hill, R., Graham, T., Ridley, J., Blaker, A., Calvert, D., Copsey, D., Ellis, R., Hewitt, H., Hyder, P., Ineson, S., Mulcahy, J., Siahaan, A., & Walton, J. (2018). The Low-Resolution Version of HadGEM3 GC3.1: Development and Evaluation for Global Climate. *Journal of Advances in Modeling Earth Systems*, *10*(11), 2865–2888. https://doi.org/10.1029/2018MS001370

Lee, S. K., Lumpkin, R., Baringer, M. O., Meinen, C. S., Goes, M., Dong, S., Lopez, H., & Yeager, S. G. (2019). Global Meridional Overturning Circulation Inferred From a Data-Constrained Ocean & Sea-Ice Model. *Geophysical Research Letters*, *46*(3), 1521–1530. https://doi.org/10.1029/2018GL080940

Li, L., Yu, Y., Tang, Y., Lin, P., Xie, J., Song, M., Dong, L., Zhou, T., Liu, L., Wang, L., Pu, Y., Chen, X., Chen, L., Xie, Z., Liu, H., Zhang, L., Huang, X., Feng, T., Zheng, W., … Wei, J. (2020). The Flexible Global Ocean-Atmosphere-Land System Model Grid-Point Version 3 (FGOALS-g3): Description and Evaluation. *Journal of Advances in Modeling Earth Systems*, *12*(9), e2019MS002012. https://doi.org/10.1029/2019MS002012

Lin, Y., Huang, X., Liang, Y., Qin, Y., Xu, S., Huang, W., Xu, F., Liu, L., Wang, Y., Peng, Y., Wang, L., Xue, W., Fu, H., Zhang, G. J., Wang, B., Li, R., Zhang, C., Lu, H., Yang, K., … Gong, P. (2020). Community Integrated Earth System Model (CIESM): Description and Evaluation. *Journal of Advances in Modeling Earth Systems*, *12*(8), e2019MS002036. https://doi.org/10.1029/2019MS002036

Lovato, T., Peano, D., Butenschön, M., Materia, S., Iovino, D., Scoccimarro, E., Fogli, P. G., Cherchi, A., Bellucci, A., Gualdi, S., Masina, S., & Navarra, A. (2022). CMIP6 Simulations With the CMCC Earth System Model (CMCC-ESM2). *Journal of Advances in Modeling Earth Systems*, *14*(3), e2021MS002814. https://doi.org/10.1029/2021MS002814

Lumpkin, R., & Speer, K. (2007). Global Ocean Meridional Overturning. *Journal of Physical Oceanography*, *37*(10), 2550–2562. https://doi.org/10.1175/JPO3130.1

Lurton, T., Balkanski, Y., Bastrikov, V., Bekki, S., Bopp, L., Braconnot, P., Brockmann, P., Cadule, P., Contoux, C., Cozic, A., Cugnet, D., Dufresne, J. L., Éthé, C., Foujols, M. A., Ghattas, J., Hauglustaine, D., Hu, R. M., Kageyama, M., Khodri, M., … Boucher, O. (2020). Implementation

of the CMIP6 Forcing Data in the IPSL-CM6A-LR Model. *Journal of Advances in Modeling Earth Systems*, *12*(4), e2019MS001940. https://doi.org/10.1029/2019MS001940

Mauritsen, T., Bader, J., Becker, T., Behrens, J., Bittner, M., Brokopf, R., Brovkin, V., Claussen, M., Crueger, T., Esch, M., Fast, I., Fiedler, S., Fläschner, D., Gayler, V., Giorgetta, M., Goll, D. S., Haak, H., Hagemann, S., Hedemann, C., … Roeckner, E. (2019). Developments in the MPI-M Earth System Model version 1.2 (MPI-ESM1.2) and Its Response to Increasing CO2. *Journal of Advances in Modeling Earth Systems*, *11*(4), 998–1038. https://doi.org/10.1029/2018MS001400

Müller, W. A., Jungclaus, J. H., Mauritsen, T., Baehr, J., Bittner, M., Budich, R., Bunzel, F., Esch, M., Ghosh, R., Haak, H., Ilyina, T., Kleine, T., Kornblueh, L., Li, H., Modali, K., Notz, D., Pohlmann, H., Roeckner, E., Stemmler, I., … Marotzke, J. (2018). A Higher-resolution Version of the Max Planck Institute Earth System Model (MPI-ESM1.2-HR). *Journal of Advances in Modeling Earth Systems*, *10*(7), 1383–1413. https://doi.org/10.1029/2017MS001217

Park, S., Shin, J., Kim, S., Oh, E., & Kim, Y. (2019). Global Climate Simulated by the Seoul National University Atmosphere Model Version 0 with a Unified Convection Scheme (SAM0-UNICON). *Journal of Climate*, *32*(10), 2917–2949. https://doi.org/10.1175/JCLI-D-18-0796.1

Séférian, R., Nabat, P., Michou, M., Saint-Martin, D., Voldoire, A., Colin, J., Decharme, B., Delire, C., Berthet, S., Chevallier, M., Sénési, S., Franchisteguy, L., Vial, J., Mallet, M., Joetzjer, E., Geoffroy, O., Guérémy, J. F., Moine, M. P., Msadek, R., … Madec, G. (2019). Evaluation of CNRM Earth System Model, CNRM-ESM2-1: Role of Earth System Processes in Present-Day and Future Climate. *Journal of Advances in Modeling Earth Systems*, *11*(12), 4182–4227. https://doi.org/10.1029/2019MS001791

Sellar, A. A., Jones, C. G., Mulcahy, J. P., Tang, Y., Yool, A., Wiltshire, A., O'Connor, F. M., Stringer, M., Hill, R., Palmieri, J., Woodward, S., de Mora, L., Kuhlbrodt, T., Rumbold, S. T., Kelley, D. I., Ellis, R., Johnson, C. E., Walton, J., Abraham, N. L., … Zerroukat, M. (2019). UKESM1: Description and Evaluation of the U.K. Earth System Model. *Journal of Advances in Modeling Earth Systems*, *11*(12), 4513–4558. https://doi.org/10.1029/2019MS001739

Swart, N. C., Cole, J. N. S., Kharin, V. v., Lazare, M., Scinocca, J. F., Gillett, N. P., Anstey, J., Arora, V., Christian, J. R., Hanna, S., Jiao, Y., Lee, W. G., Majaess, F., Saenko, O. A., Seiler, C., Seinen, C., Shao, A., Sigmond, M., Solheim, L., … Winter, B. (2019). The Canadian Earth System Model version 5 (CanESM5.0.3). *Geoscientific Model Development*, *12*(11), 4823–4873. https://doi.org/10.5194/GMD-12-4823-2019

Tatebe, H., Ogura, T., Nitta, T., Komuro, Y., Ogochi, K., Takemura, T., Sudo, K., Sekiguchi, M., Abe, M., Saito, F., Chikira, M., Watanabe, S., Mori, M., Hirota, N., Kawatani, Y., Mochizuki, T., Yoshimura, K., Takata, K., O'Ishi, R., … Kimoto, M. (2019). Description and basic evaluation of simulated mean state, internal variability, and climate sensitivity in MIROC6. *Geoscientific Model Development*, *12*(7), 2727–2765. https://doi.org/10.5194/GMD-12-2727-2019

Tjiputra, J. F., Schwinger, J., Bentsen, M., L. Morée, A., Gao, S., Bethke, I., Heinze, C., Goris, N., Gupta, A., He, Y. C., Olivié, D., Seland, O., & Schulz, M. (2020). Ocean biogeochemistry in the Norwegian Earth System Model version 2 (NorESM2). *Geoscientific Model Development*, *13*(5), 2393–2431. https://doi.org/10.5194/GMD-13-2393-2020

Voldoire, A., Saint-Martin, D., Sénési, S., Decharme, B., Alias, A., Chevallier, M., Colin, J., Guérémy, J. F., Michou, M., Moine, M. P., Nabat, P., Roehrig, R., Salas y Mélia, D., Séférian, R., Valcke, S.,

Beau, I., Belamari, S., Berthet, S., Cassou, C., … Waldman, R. (2019). Evaluation of CMIP6 DECK Experiments With CNRM-CM6-1. *Journal of Advances in Modeling Earth Systems*, *11*(7), 2177–2213. https://doi.org/10.1029/2019MS001683

Volodin, E., & Gritsun, A. (2018). Simulation of observed climate changes in 1850-2014 with climate model INM-CM5. *Earth Syst. Dynam*, *9*, 1235–1242. https://doi.org/10.5194/esd-9-1235-2018

Volodin, E. M., Mortikov, E. v., Kostrykin, S. v., Galin, V. Y., Lykossov, V. N., Gritsun, A. S., Diansky, N. A., Gusev, A. v., Iakovlev, N. G., Shestakova, A. A., & Emelina, S. v. (2018). Simulation of the modern climate using the INM-CM48 climate model. *Russian Journal of Numerical Analysis and Mathematical Modelling*, *33*(6), 367–374. https://doi.org/10.1515/RNAM-2018-0032/MACHINEREADABLECITATION/RIS

Williams, K. D., Copsey, D., Blockley, E. W., Bodas-Salcedo, A., Calvert, D., Comer, R., Davis, P., Graham, T., Hewitt, H. T., Hill, R., Hyder, P., Ineson, S., Johns, T. C., Keen, A. B., Lee, R. W., Megann, A., Milton, S. F., Rae, J. G. L., Roberts, M. J., … Xavier, P. K. (2018). The Met Office Global Coupled Model 3.0 and 3.1 (GC3.0 and GC3.1) Configurations. *Journal of Advances in Modeling Earth Systems*, *10*(2), 357–380. https://doi.org/10.1002/2017MS001115

Wyser, K., van Noije, T., Yang, S., von Hardenberg, J., O'Donnell, D., & Döscher, R. (2020). On the increased climate sensitivity in the EC-Earth model from CMIP5 to CMIP6. *Geoscientific Model Development*, *13*(8), 3465–3474. https://doi.org/10.5194/GMD-13-3465-2020

Yukimoto, S., Kawai, H., Koshiro, T., Oshima, N., Yoshida, K., Urakawa, S., Tsujino, H., Deushi, M., Tanaka, T., Hosaka, M., Yabu, S., Yoshimura, H., Shindo, E., Mizuta, R., Obata, A., Adachi, Y., & Ishii, M. (2019). The Meteorological Research Institute Earth System Model Version 2.0, MRI-ESM2.0: Description and Basic Evaluation of the Physical Component. *Journal of the Meteorological Society of Japan. Ser. II*, *97*(5), 931–965. https://doi.org/10.2151/JMSJ.2019-051

Zhang, H., Zhang, M., Jin, J., Fei, K., Ji, D., Wu, C., Zhu, J., He, J., Chai, Z., Xie, J., Dong, X., Zhang, D., Bi, X., Cao, H., Chen, H., Chen, K., Chen, X., Gao, X., Hao, H., … Zhu, J. (2020). Description and Climate Simulation Performance of CAS-ESM Version 2. *Journal of Advances in Modeling Earth Systems*, *12*(12), e2020MS002210. https://doi.org/10.1029/2020MS002210

Ziehn, T., Chamberlain, M. A., Law, R. M., Lenton, A., Bodman, R. W., Dix, M., Stevens, L., Wang, Y. P., & Srbinovsky, J. (2020). The Australian Earth System Model: ACCESS-ESM1.5. *Journal of Southern Hemisphere Earth Systems Science*, *70*(1), 193–214. https://doi.org/10.1071/ES19035

Ziehn, T., Lenton, A., Law, R. M., Matear, R. J., & Chamberlain, M. A. (2017). The carbon cycle in the Australian Community Climate and Earth System Simulator (ACCESS-ESM1) - Part 2: Historical simulations. *Geoscientific Model Development*, *10*(7), 2591–2614. https://doi.org/10.5194/GMD-10-2591-2017

Moat, B. I., Frajka-Williams, E., Smeed, D. A., Rayner, D., Johns, W. E., Baringer, M. O., et al. (2022). Atlantic meridional overturning circulation observed by the RAPID-MOCHA-WBTS (RAPID-Meridional Overturning Circulation and Heatflux Array-Western Boundary Time Series) array at 26N from 2004 to 2020 (v2020.2). [Dataset]. British Oceanographic Data Centre, Natural Environment Research Council. https://doi.org/10.5285/e91b10af-6f0a-7fa7-e053-6c86abc05a09